JOURNAL OF GEOPHYSICAL RESEARCH: OCEANS, VOL. 119, 572–594, doi:10.1002/2013JC009441, 2014

Polynya dynamics drive primary production in the Larsen A and B embayments following ice shelf collapse

Mattias R. Cape,[1] Maria Vernet,[1] Mati Kahru,[1] and Gunnar Spreen[2]

Received 13 September 2013; revised 25 November 2013; accepted 12 December 2013; published 28 January 2014.

[1] The climate-driven collapses of the Larsen A and B ice shelves have opened up new regions of the coastal Antarctic to the influence of sea ice resulting in increases in seasonal primary production. In this study, passive microwave remote sensing of sea ice concentration and satellite imagery of ocean color are employed to quantify the magnitude of and variability in open water area and net primary productivity (NPP) in the Larsen embayments between 1997 and 2011. Numerical model output provides context to analyze atmospheric forcing on the coastal ocean. Following ice shelf disintegration the embayments function as coastal, sensible heat polynyas. The Larsen A and B are as productive as other Antarctic shelf regions, with seasonally averaged daily NPP rates reaching 1232 and 1127 mg C m^{-2} d^{-1} and annual rates reaching 200 and 184 g C m^{-2} yr^{-1}, respectively. A persistent cross-shelf gradient in NPP is present with higher productivity rates offshore, contrasting with patterns observed along the West Antarctic Peninsula. Embayment productivity is intimately tied to sea ice dynamics, with large interannual variability in NPP rates driven by open water area and the timing of embayment opening. Opening of the embayment is linked to periods of positive Southern Annular Mode and stronger westerlies, which lead to the vertical deflection of warm, maritime air over the peninsula and down the leeward side causing increases in surface air temperature and wind velocity. High productivity in these new polynyas is likely to have ramifications for organic matter export and marine ecosystem evolution.

Citation: Cape, M. R., M. Vernet, M. Kahru, and G. Spreen (2014), Polynya dynamics drive primary production in the Larsen A and B embayments following ice-shelf collapse, *J. Geophys. Res. Oceans*, *119*, 572–594, doi:10.1002/2013JC009441.

1. Introduction

[2] In the past 50 years, the Antarctic Peninsula (AP) has undergone rapid regional climate change, with a warming of both air and sea that has significantly impacted cryosphere dynamics [*Vaughan and Doake*, 1996; *Cook et al*., 2005; *Marshall et al*., 2006; *Cook and Vaughan*, 2010; *Stammerjohn et al*., 2012]. Stronger westerly winds associated with a positive Southern Annular Mode (SAM) are thought to have contributed to increases in air temperature and meltwater fluxes along the northeast Antarctic Peninsula, ultimately leading to the collapse of both the Larsen A and B ice shelves [*Skvarca et al*., 1999; *Thompson*, 2002; *Orr et al*., 2004; *Scambos et al*., 2004; *van den Broeke et al*., 2005]. These events precipitated changes in cryosphere-ocean dynamics in the NW Weddell Sea, including the acceleration of coastal glaciers [*Rott et al*., 2002; *Glasser et al*., 2011], and possibly changes in coastal ocean circulation and sedimentation rates as well as the opening of large coastal regions to the influence of sea ice.

[3] The Larsen A ice shelf, continuously present since the Little Ice Age approximately 600 years before present after advancing and retreating three times during the Holocene [*Brachfeld et al*., 2003], covered approximately 4000 km^2 in 1961 but retreated incrementally until January–February 1995, when the final major collapse of the ice shelf occurred [*Rott et al*., 1996]. The Larsen B ice shelf, which had been present throughout the Holocene (approximately 10,000 years) [*Domack et al*., 2005], covered 12,000 km^2 in 1963 and continued to advance until the early 1990s [*Ferrigno et al*., 2008a; *Cook and Vaughan*, 2010]. It then proceeded to retreat much like the Larsen A until 2002 when 3250 km^2 of the ice shelf disintegrated [*Scambos et al*., 2000, 2003].

[4] The Larsen embayments are now transitioning to a more dynamic state as part of the seasonal sea ice zone [*Tréguer and Jacques*, 1992]. Structuring the timing, magnitude, and spatial extent of blooms, sea ice serves as a major physical forcing on phytoplankton at these latitudes [*Smith et al*., 1995; *Stammerjohn et al*., 2012]. Once permanently dark waters are now seasonally exposed to the atmosphere and solar irradiance in the absence of heavy ice

Additional supporting information may be found in the online version of this article.

[1]Scripps Institution of Oceanography, University of California, San Diego, California, USA.
[2]Norwegian Polar Institute, Fram Centre, Tromsø, Norway.

Corresponding author: M. R. Cape, Scripps Institution of Oceanography, University of California, San Diego, 9500 Gilman Drive MC 0218, La Jolla, CA 92093-0218, USA. (mcape@ucsd.edu)

2169-9275/14/10.1002/2013JC009441

cover, making phytoplankton growth possible. Within the sea ice zone, primary production can be limited by light [*Mitchell et al*., 1991], micronutrient availability [*Martin et al*., 1990b; *Boyd*, 2004; *Boyd and Ellwood*, 2010] or zooplankton grazing [*Walsh et al*., 2001]. Along the coastal Antarctic Peninsula, where macro and micronutrients are thought abundant [*Martin et al*., 1990a], phytoplankton blooms and spatial gradients in primary productivity may be controlled by water column stability primarily via freshwater input from coastal glaciers and sea ice melt [*Smith and Nelson*, 1986; *Mitchell et al*., 1991; *Tréguer and Jacques*, 1992; *Klinck*, 1998; *Dierssen et al*., 2002; *Garibotti et al*., 2003]. Shallow summer mixed layers, along with the potential seeding of the water column by sea ice algae as the ice retreats, can enhance phytoplankton growth [*Ackley and Sullivan*, 1994]. Similar dynamics are thought to occur along the eastern Antarctic Peninsula (EAP) where in the absence of the ice shelf, freshwater from the tidewater glacier is expected to spread along the sea surface during the spring and summer, increasing stratification (A. Gordon, personal communication). Melting of retreating sea ice would reinforce this stratification, and during the period of highest air temperature and incident light in the summer, could be conducive to phytoplankton growth.

[5] Despite extensive seasonal ice cover and relatively low average rates of annual net primary productivity [*Arrigo et al*., 2008a], biological production in the Southern Ocean is thought to play an important role in the drawdown of CO_2 into the deep ocean via the meridional overturning circulation [*Takahashi et al*., 2009]. This is especially the case along the continental shelves surrounding Antarctica, where intense phytoplankton blooms and comparatively high levels of primary production occur during the summer [*Arrigo et al*., 2008b]. The seasonal presence of phytoplankton as a potential new source of organic carbon marks an abrupt change in the marine ecosystem, which is hypothesized to increase carbon export to the deep ocean and potentially serve as a negative feedback to climate change [*Bertolin and Schloss*, 2009; *Peck et al*., 2010; *Shadwick et al*., 2013].

[6] While the ecological effects of atmospheric warming and changes in the seasonality of sea ice cover are well documented along the open West Antarctic Peninsula (WAP) shelf [*Stammerjohn et al*., 2008; *Vernet et al*., 2008; *Montes-Hugo et al*., 2009], few studies have been undertaken along the AP's eastern coastline [*Bertolin and Schloss*, 2009; *Gutt et al*., 2011, 2013; *Sane et al*., 2011b, 2012, 2013]. These new waters now appear to be biologically active, perhaps contributing significantly to Weddell Sea production on an otherwise ice-covered continental shelf. Sedimentation in the Weddell Sea can be very high (1200 mg C m^2 d^{-1}), with as much as 8–15% of daily primary production caught in sediment traps [*Froneman et al*., 2004]. This downward carbon flux depends on grazer community structure and phytoplankton cell-size distribution [*Fischer et al*., 2002]. This new state of the cryosphere along the EAP may therefore have important consequences for habitat use by higher trophic levels and the evolution of the benthic communities below the former ice shelves [*Gutt et al*., 2011, 2013].

[7] Following the demise of the ice shelves, we hypothesized that the previously ice-covered waters of the Larsen B embayment now support a thriving photosynthetic autotrophic community, with production rates similar to other productive areas of the Weddell Sea. We also expected that sea ice would be a major physical forcing on phytoplankton growth by both limiting the area over which production can occur and temporally constraining production depending on the timing of retreat. In this study we address the following questions: (1) what are the long-term patterns of phytoplankton production in the Larsen embayments, (2) how do spatial and temporal patterns of phytoplankton relate to fluctuations in sea ice cover and open water area, (3) how do sea ice dynamics relate to atmospheric conditions and climate forcing, and (4) are the Larsen embayments important sites for carbon fixation and potentially export? For this purpose we analyze remote sensing data for ocean color and sea ice concentration combined with atmospheric reanalysis data sets between 1997 and 2011 to describe phytoplankton variability in relation to environmental forcing. In doing so, we give the first estimate of interannual water column phytoplankton production for these embayments, thereby evaluating the possible contribution of this new production to carbon export and providing a baseline for future marine ecosystem studies of the NW Weddell Sea.

2. Methods

2.1. Study Area

[8] The Larsen A and B embayments lie in the Northwest Weddell Sea, near the tip of the Antarctic Peninsula. In order to characterize spatiotemporal variability in phytoplankton in this region we considered three sectors (Figure 1). These included the Larsen A (4262 km^2) and Larsen B (7473 km^2) embayments separately as well as a larger sector within the coastal Northwest Weddell Sea (91,049 km^2). We defined the western boundary of these regions by the Antarctic coastline using the most recent Mosaic of Antarctica provided by NSIDC (MOA, http://nsidc.org/data/moa/, [*Scambos et al*., 2007]), modified using a 1997–2011 ocean color composite to account for the further retreat of the ice shelves since the compilation of MOA in 2006. The Larsen A embayment was delimited to the east by a line joining the tip of Cape Longing and Robertson Island, which corresponds approximately to the extent of the ice shelf in 1961 [*Ferrigno et al*., 2008b]. Similarly, the eastern boundary of the Larsen B embayment was defined by a line joining the tips of Cape Framnes and Robertson Island, corresponding to the ice shelf extent in 1995 [*Ferrigno et al*., 2008a]. The NW Weddell Sea region extends from 63.5°S to 68°S and 56°W to the East. Satellite data sets were mapped to an equal-area projection with a pixel size of 1 km^2 encompassing 60° to 68°S and 50°W to 68°W. While the Larsen A ice shelf had retreated almost to its final position by 1997, the start of this study, the Larsen B experienced further retreat in 1999, 2000, and 2002. Presence of this remaining ice shelf is therefore taken into account in the analyses below.

2.2. Net Primary Productivity (NPP)

[9] Net primary productivity for the period of October–March 1997–2011 (late spring-early fall, termed seasonal in the remainder of the manuscript) was calculated using

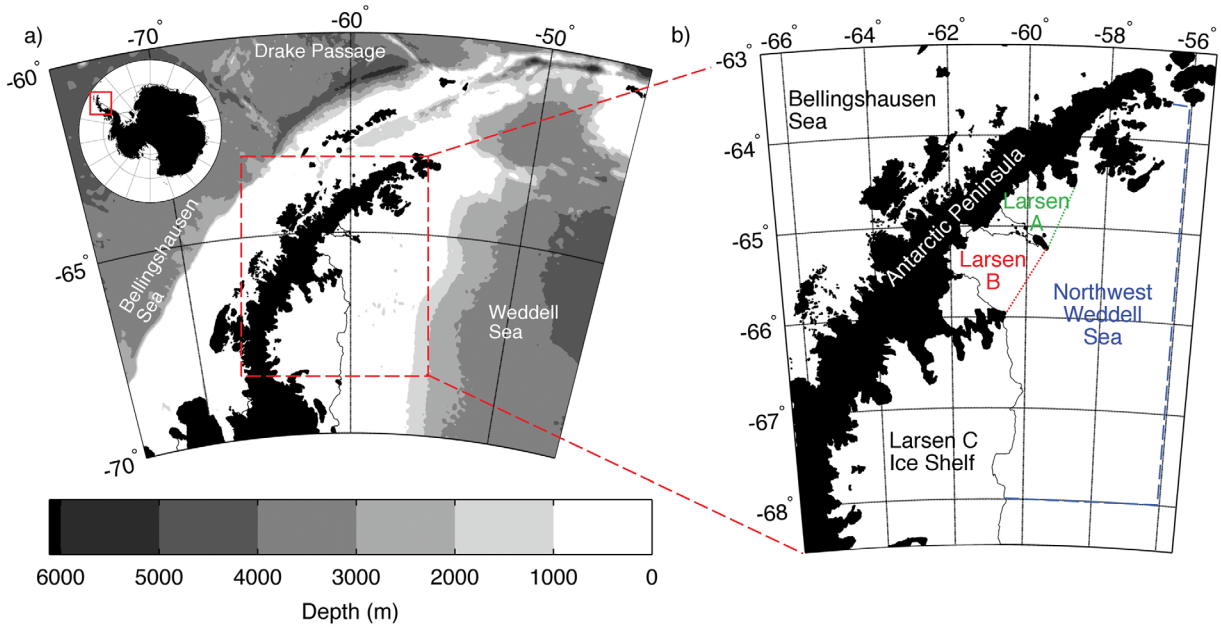

Figure 1. Map of the study area depicting (a) the Antarctic Peninsula and (b) the study area along the northwest Weddell Sea. The shelf in this region is 200–300 km wide with an average depth between 500 and 600 m. Areas over which statistics were calculated for the three regions of interest (NW Weddell Sea, Larsen A, and Larsen B embayments) are outlined. Coastlines are taken from *Scambos et al*. [2007] and bathymetry from *Smith and Sandwell* [1997].

satellite-derived daily images of chlorophyll-a and photosynthetically available radiation as inputs into a depth-integrated primary production model [*Dierssen et al*., 2000]. This model uses the structure of the standard Vertically Generalized Production Model (VGPM) [*Behrenfeld and Falkowski*, 1997] to calculate net primary productivity in the euphotic zone (NPP) based on a photoadaptive variable (P^B_{opt}), daylength (D), surface chlorophyll-a concentration measured via satellite (C_{sat}), euphotic-zone depth (Z_{eu}), and an irradiance-dependent function (F):

$$NPP = P^B_{opt} D C_{sat} Z_{eu} F \tag{1}$$

Coefficients for the model have been parameterized to field data collected from the West Antarctic Peninsula [*Dierssen et al*., 2000], with

$$F = \frac{E_d(0^+)}{E_d(0^+) + 11.7} \tag{2}$$

$$Z_{eu} = 48.8 C_{sat}^{-0.36} \tag{3}$$

$$P^B_{opt} = 1.09\ mg\ C\ mg\ \text{chl}^{-1}\ h^{-1} \tag{4}$$

E_d0^+ corresponds to satellite-derived photosynthetically available radiation. Daily and monthly maps were generated for further analysis. Details on individual inputs to the model appear below.

[10] We generated a time series of daily, depth integrated NPP by averaging all available cloud-free pixels within each region in daily images. The mean, seasonally averaged proportion of days with valid satellite data within the embayments was 22% with significant interannual variability due primarily to variability in sea ice and cloud cover (minimum 0%, maximum 50%). For days with no valid data, linear interpolation using neighboring points was used to estimate NPP. Annual primary productivity was then calculated by integrating the daily time series over the 1 October to 31 March period for each season and within each region. Similarly, total annual primary production was estimated by multiplying the estimated daily depth integrated NPP by daily open water extent, and integrating over each season.

2.3. Chlorophyll-a (chl-a)

[11] Daily maps of surface chl-a concentrations were generated from ocean color data collected by MODIS Aqua (R2012.0) and SeaWiFS (R2010.0) and distributed by NASA (http://oceancolor.gsfc.nasa.gov). Chl-a concentrations were calculated using the maximum band-ratio algorithms for MODIS (OC3M) and SeaWiFS (OC4v4) [*O'Reilly et al*., 1998, 2000]. Because extensive changes in the Antarctic coastline due to ice shelf collapse have not been integrated in the standard NASA ocean color processing, land masks erroneously omit valid pixels within approximately 120 km of the coast in regions previously covered by ice shelf. Therefore, we generated images of chl-a concentration at 1 km resolution for the Larsen A and B regions by reprocessing L1A data to L2 using the standard ocean color processing flags in SeaDAS (http://seadas.gsfc.nasa.gov) omitting the land mask. This data set was merged with L2 daily chl-a images using Windows Image Manager (WIM) software (http://www.wimsoft.com) for the wider Antarctic Peninsula to generate daily, regional maps at 1 km resolution over the entire study area.

2.4. Photosynthetically Available Radiation (PAR)

[12] PAR was calculated from MODIS and SeaWiFS using standard NASA algorithms. Daily, merged composites at 1 km resolution were generated from both reprocessed L1A and L2 data sets following the processing scheme outlined for chl-a. These images were then spatially binned to 9 km resolution.

2.5. Sea Ice Concentration and Open Water Area

[13] As with ocean color processing, standard sea ice products fail to integrate recent changes to the Antarctic coastline caused by the retreat of ice shelves. In this study, daily measurements of sea ice concentration on a 6.25 km grid were calculated from the 89 GHz channel of the Advanced Microwave Scanning Radiometer-Earth Observing System (AMSR-E) sensor (University of Hamburg, ftp://ftp-projects.zmaw.de/seaice/AMSR-E_ASI_IceConc/tmp_no_landmask/). To complement the time series prior to the launch of AMSR-E in June 2002, we used the lower resolution (12.5 km grid) Special Sensor Microwave Imager (SSM/I) 85 GHz bands. In both cases, sea ice concentration was calculated using the ARTIST (Arctic Radiation and Turbulence Interaction STudy) Sea Ice (ASI) algorithm [*Kaleschke et al*., 2001; *Spreen et al*., 2008], which yields ice concentration at higher spatial resolution compared to other standard algorithms (e.g., NASA-Team algorithm).

[14] Previous studies have shown that biases in the calculation of sea ice concentration may result from using different processing algorithms [*Andersen et al*., 2007]. Furthermore, differences in sensor spatial resolution can lead to biases in absolute concentration calculations, particularly near shore where signal from ice-covered land can lead to overestimation of sea ice concentration [*Kern et al*., 2007; *Maaß and Kaleschke*, 2010]. Instead of using absolute concentration, we calculated open water area based on thresholds of sea ice concentration to estimate the area available for water column primary production. This technique has been used in previous studies and is less sensitive to the algorithm used in the calculation of ice concentration [*Comiso and Parkinson*, 2008]. Because of the different sensor resolutions, we used two different thresholds to estimate open water. Individual pixels were considered open water when sea ice concentration fell below 15% for AMSR-E and 40% for SSM/I. We settled upon different thresholds after comparing the records over the 2002–2011 period of sensor overlap, using the 15% threshold on AMSR-E as a reference data set. We ensured there were no significant differences in seasonal cycles, phase, or amplitude, and that bias between the time series was minimized (see supporting information). Maps of ice cover processed using this scheme were then used to create time series of daily open water area by summing open water pixels falling within each region. From these we also created seasonal maps of the total number of open water days by summing the number of days when each pixel could be considered ice-free between October 1 and March 31. Scattered ice floes or very thin ice may still be present in these "ice-free" regions due to ice concentrations falling below the thresholds and errors in the ice concentration algorithm. However, during the periods classified as "ice-free," sufficient open water will always be present to allow primary production.

2.6. Reanalysis Products

[15] We obtained numerically analyzed monthly atmospheric data sets from the European Center for Medium-Range Weather Forecasts ERA-Interim data set (EMCWF, http://www.ecmwf.int). The data sets use a horizontal grid spacing of approximately 80 km and include surface wind (at 10 m), surface pressure and temperature (at 2 m) as well as geopotential height at 500 and 850 hPa vertical wind velocities. The pressure surface at 850 hPA corresponds approximately to the summit of the Antarctic Peninsula near the Larsen B embayment. Monthly anomalies for these variables were calculated by subtracting the monthly 1997–2011 climatology from monthly maps. Following the approach of *van Lipzig et al*. [2008] and others, we reduced the monthly anomaly time series to two composites (averages) for the 8 months with the largest and smallest mean open water areas in the Larsen A and B embayments to describe typical, anomalous atmospheric circulation patterns associated with extremes in sea ice cover. We then calculated the difference between high and low composites to identify factors that may contribute to the opening of the embayments.

2.7. SAM Index

[16] We used the observation-based index provided by Garreth Marshall (http://www.nerc-bas.ac.uk/icd/gjma/sam.html) to characterize the state of the SAM, a dominant mode of climate variability along the Antarctic Peninsula [*Marshall*, 2003, 2006]. Positive SAM values correspond to negative atmospheric pressure anomalies at high latitudes and positive anomalies at low latitude.

2.8. Data Analysis

[17] We used the first (last) date where open water area exceeded 15% of the Larsen A and Larsen B embayment areas for three consecutive days between 1 October and 31 March to identify the opening (closing) date of the embayments. Following *Stammerjohn et al*. [2008], we defined three statistics: open water duration, open water days, and persistence. Open water duration equates to the number of days between the opening and closing date of the embayment. Open water days refer to the number of days between these dates where open water area exceeds the 15% threshold. Open water days can be shorter than open water duration if sea ice advances and retreats more than once between the opening and closing dates. Persistence was then calculated by dividing open water days by open water duration, which gives the percentage of time the embayments were open within the total open water season. Similarly, we defined the start (end) of the phytoplankton growth period by considering the first (last) date when mean NPP in the embayments exceeded (fell below) 0.5 g C m^{-2} d^{-1} for three consecutive days. This corresponded approximately to the date when chl-a concentration in surface waters exceeded 1 mg m^{-3}. We refer to these dates as defining the timing of phytoplankton blooms in the remainder of this manuscript. Bloom duration corresponds to the number of days between the start and end dates, while bloom days equals the number of days between bloom start and end where NPP exceeded the bloom threshold.

Table 1. Open Water Characteristics for the Larsen A and B Embayments[a]

	Larsen A					Larsen B				
Year	Opening (DOY)	Closing (DOY)	Duration (days)	Open Water Days (days)	Persistence (%)	Opening (DOY)	Closing (DOY)	Duration (days)	Open Water Days (days)	Persistence (%)
1997–1998	–	–	0	0	–	–	–	0	0	–
1998–1999	336	446	110	84	76	336	445	109	44	40
1999–2000	368	446	78	72	92	283	404	121	64	53
2000–2001	–	–	0	0	–	–	–	0	0	–
2001–2002	275	454	179	179	100	272	421	149	139	93
2002–2003	349	460	111	80	72	–	–	0	0	–
2003–2004	437	442	6	6	100	439	441	3	3	100
2004–2005	279	449	170	152	89	277	438	161	129	80
2005–2006	301	459	158	112	71	278	438	160	116	73
2006–2007	302	446	144	131	91	302	423	121	116	96
2007–2008	–	–	0	0	–	–	–	0	0	–
2008–2009	325	447	122	118	97	333	445	112	104	93
2009–2010	–	–	0	0	–	281	286	5	5	100
2010–2011	296	442	146	146	100	301	431	130	97	75
Mean	326.80	449.10	87.43	77.14	88.87	310.20	417.20	76.50	58.36	80.25
SD	49.01	6.45	71.45	65.31	11.60	50.68	47.85	69.30	56.49	20.50

[a]Opening and closing dates listed as day of the year (DOY), with January 1 = 1 and December 31 as 365 (nonleap) or 366 (leap year). Because seasons span >1 year, the opening and closing dates can exceed 365 or 366. For example, an opening day of January 1 would correspond to day of the year 367 if the prior year was a leap year. A dash (–) indicates no data.

Persistence was calculated by dividing bloom days by bloom duration.

[18] Two transects were also created in the Larsen A (from 60.34°W, 64.627°S to 53.137°W, 65.753°S) and the Larsen B (from 61.549°W, 65.231°S to 52.826°W, 66.698°S) to examine cross-shelf patterns of primary production. NPP along the transect was calculated using a monthly data set by taking a mean and standard deviation of all valid pixels in a 3 × 3 pixel box surrounding each point along the transect. Neighboring transect points were separated by approximately 1 km.

[19] Results are presented as mean ± one standard deviation unless otherwise stated. The correlation between two variables was calculated using Spearman's Rank-Order Correlation, and reported as $\rho(\mathrm{df}) = \rho$ coefficient, p value, where df = N-2 and N = number of pairwise cases. Simple linear regression was used as a first order estimate of trends in the data, with results presented as b = regression coefficient when significant, $t_{(df)}$ = t-statistic, p-value, where df = N-2 as above. Statistics were calculated using MATLAB Release 2013a (The MathWorks, Inc., Natick, Massachusetts, USA).

3. Results

3.1. Patterns of Sea Ice and Open Water

3.1.1. Seasonal and Interannual Patterns

[20] *Larsen A:* While the onset of seasonal open water development exhibits little interannual consistency, with initial increases occurring anywhere between 2 October (2001–2002) and 13 March (2003–2004), peak values of open water area tend to occur in January before a rapid decline in March (Table 1 and Figure 2). On average, the embayment opens on November 22 (± 49.01 days) and closes on March 24 (± 6.45 days), leading to an average open water duration of 87.43 ± 71.45 days. Open water conditions often do not persist throughout a season, with sea ice cover fluctuating rapidly on the time scale of days. An extreme example can be seen in mid-March 2004, when the Larsen A opened to a maximum size of 2400 km^2 (approximately 56% of the total embayment) over 3 days and rapidly closed over the next 3, leading to a 6 day open water season. Mean open water persistence for years when the embayment is open nevertheless remains high (88.87 ± 11.60%). There is no significant trend in embayment opening date ($t_{(8)} = -0.94$, $p = 0.38$), closing date ($t_{(8)} = -0.56$, $p = 0.59$), or open water duration ($t_{(12)} = 0.55$, $p = 0.59$) between 1997 and 2011. However, open water duration is strongly negatively correlated with the opening date of the embayment ($\rho(8) = -0.98$, $p \ll 0.001$), indicating that long open water duration tends to occur when sea ice retreats early in the season.

[21] Open water area between October and March averages 1092.48 ± 1042.83 km^2 (Table 2), with mean seasonal area ranging from 1 km^2 (1997–1998) to 3092 km^2 (2001–2002). Maximum daily open water area also occurred in 2001–2002 (4011 km^2, Figure 2), coinciding with the disintegration of the remainder of the Larsen B ice shelf and a low in NW Weddell sea ice cover (Table 2). However, several seasons (1997–1998, 2000–2001, 2007–2008, and 2009–2010) saw no significant opening of the embayment, leading to a pattern where sea ice cover and open water alternate over a 1–3 years period. With this high level of interannual variability, we find no significant trend in mean seasonal open water area overall ($t_{(12)} = 0.51$, $p = 0.62$). Mean October–March open water area is, however, negatively correlated with the opening date of the embayment ($\rho(8) = -0.88$, $p < 0.01$).

[22] *Larsen B:* Due to progressive ice shelf retreat, changes in open water area between 1997 and 2002 in the Larsen B embayment account for both changes in sea ice cover and the removal of permanent ice shelf. Opening of the embayment generally occurs in early November (November 6 ± 50.68 days) and closing in mid March

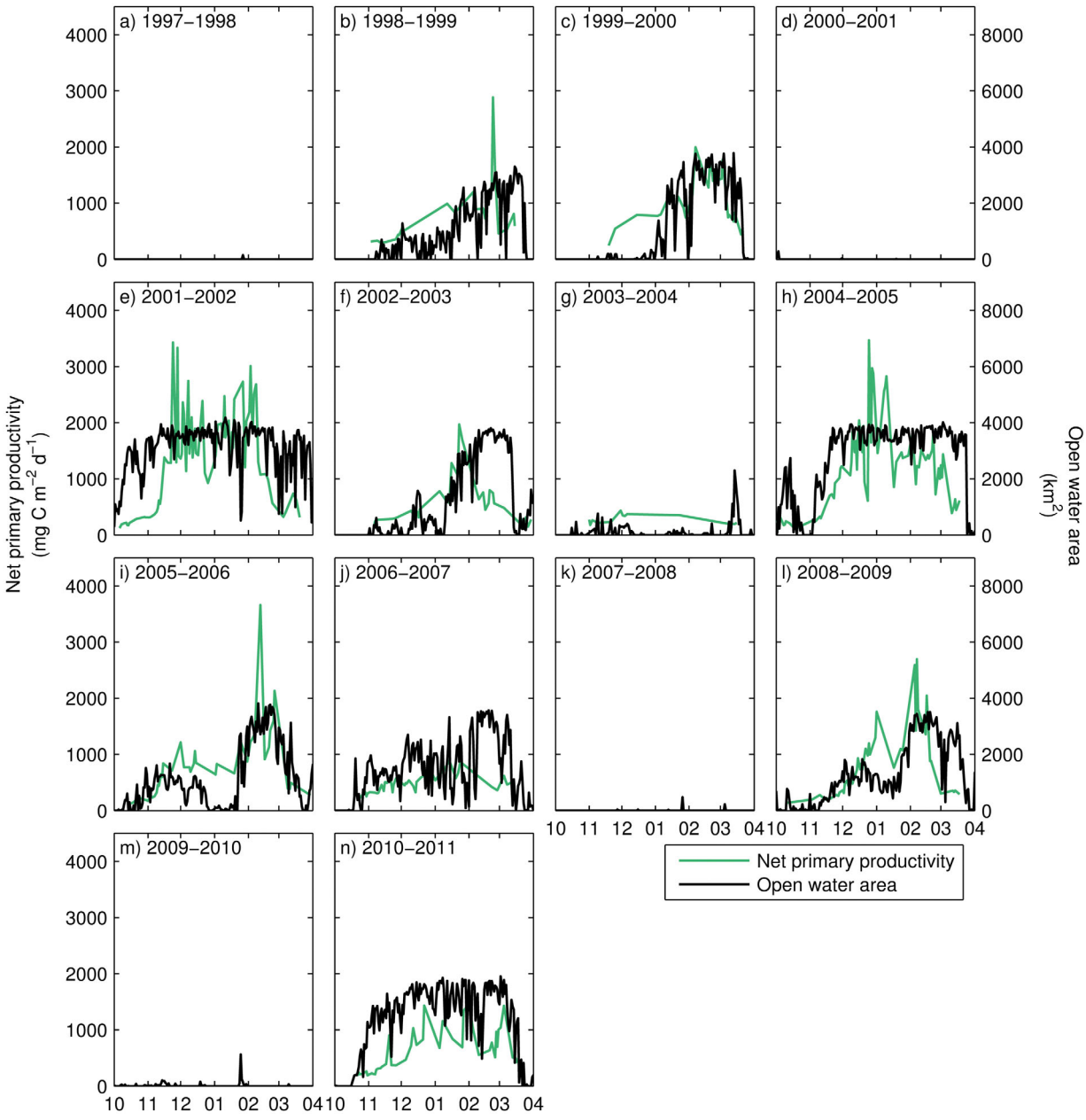

Figure 2. Seasonal time series of open water (km^2) area and net primary productivity (mg C m^{-2} d^{-1}) for the Larsen A embayment between 1997 and 2011. Plotted values represent daily averages within the Larsen A region, as indicated in Figure 1.

(February 21 ± 47.85 days), leading to shorter open water duration than the Larsen A on average (76.50 ± 69.30 days, Table 1 and Figure 3). The closing date of this embayment appears far more variable than the Larsen A (February 21 ± 47.85 days), although this variability is primarily due to one anomalous season (2009–2010). Overall opening dates for the embayment range from September 29 (2001–2002) to March 15 (2003–2004), while closing dates range from 13 October (2009–2010) to 21 March (1998–1999 and 2008–2009). Markedly short open water seasons occurred in 2003–2004 and 2008–2009, when the embayment stayed open only 3 and 5 days, respectively. Much like in the Larsen A embayment, open water conditions are persistent between October and March, averaging 80.25 ± 20.50%. Neither embayment opening date ($t_{(8)} = -0.29$, $p = 0.78$), closing date ($t_{(8)} = -0.95$, $p = 0.37$), nor open water duration exhibits any significant trend ($t_{(12)} = 0.45$, $p = 0.66$). Like the Larsen A, open water duration is negatively correlated with the opening date of the embayment ($\rho(8) = -0.76$, $p < 0.05$), though the relation is somewhat weaker.

[23] Mean open water area between October and March ranges between 2 km^2 in 2000–2001 and 3343 km^2 in 2004–2005, averaging 1297.82 ± 1336.69 km^2 overall (Table 2). Reversals in sea ice cover over time scales of days–weeks sometimes lead to multiple peaks

Table 2. Seasonal Sea Ice and Primary Production Statistics for the Larsen A, Larsen B, and NW Weddell Sea[a]

	Larsen A (4264 km^2)				Larsen B (7473 km^2)				NW Weddell (91,049 km^2)			
		Primary Production				Primary Production				Primary Production		
Year	Open Water Area (km^2)	Daily (mg C m^{-2} d^{-1})	Annual (g C m^{-2} yr^{-1})	Total Annual (Tg C yr^{-1})	Open Water Area (km^2)	Daily (mg C m^{-2} d^{-1})	Annual (g C m^{-2} yr^{-1})	Total Annual (Tg C yr^{-1})	Open Water Area (km^2)	Daily (mg C m^{-2} d^{-1})	Annual (g C m^{-2} yr^{-1})	Total Annual (Tg C yr^{-1})
1997–1998	1	0	0	0	34	0	0	0	1531	490 ± 240	54	0.121
1998–1999	918	856 ± 580	99	0.128	552	592 ± 272	91	0.059	11,726	881 ± 626	134	1.797
1999–2000	1084	884 ± 493	120	0.239	904	880 ± 555	116	0.193	16,492	1115 ± 743	191	4.157
2000–2001	3	0	0	0	2	0	0	0	1194	415 ± 196	63	0.099
2001–2002	3092	1232 ± 870	200	0.679	2443	1013 ± 737	169	0.458	56,327	1162 ± 884	199	12.901
2002–2003	1125	537 ± 398	86	0.151	66	268 ± 141	45	0.004	13,102	526 ± 328	78	1.366
2003–2004	118	259 ± 129	42	0.005	84	243 ± 101	43	0.003	3526	440 ± 276	77	0.286
2004–2005	2745	1118 ± 770	177	0.606	3343	1127 ± 867	167	0.818	20,571	990 ± 794	167	4.541
2005–2006	1118	747 ± 671	137	0.232	2152	976 ± 843	184	0.607	13,791	953 ± 674	169	2.827
2006–2007	1459	486 ± 169	77	0.137	2870	557 ± 285	77	0.335	17,920	545 ± 297	93	2.079
2007–2008	5	0	0	0	42	0	0	0	3870	633 ± 660	98	0.480
2008–2009	1269	797 ± 637	120	0.222	2967	930 ± 759	136	0.673	21,565	824 ± 720	153	4.703
2009–2010	20	0	0	0	95	0	0	0	2970	313 ± 197	59	0.192
2010–2011	2338	589 ± 395	106	0.323	2617	631 ± 369	114	0.404	20,635	656 ± 453	122	3.138
Mean	1092.48	806.26	83.24	0.195	1297.82	825.82	81.60	0.254	14658.48	788.00	118.37	2.763
SD	1042.83	668.21	67.07	0.219	1336.69	699.96	68.06	0.293	14172.06	664.40	50.59	3.365

[a]Data are presented as mean or mean ± one standard deviation.

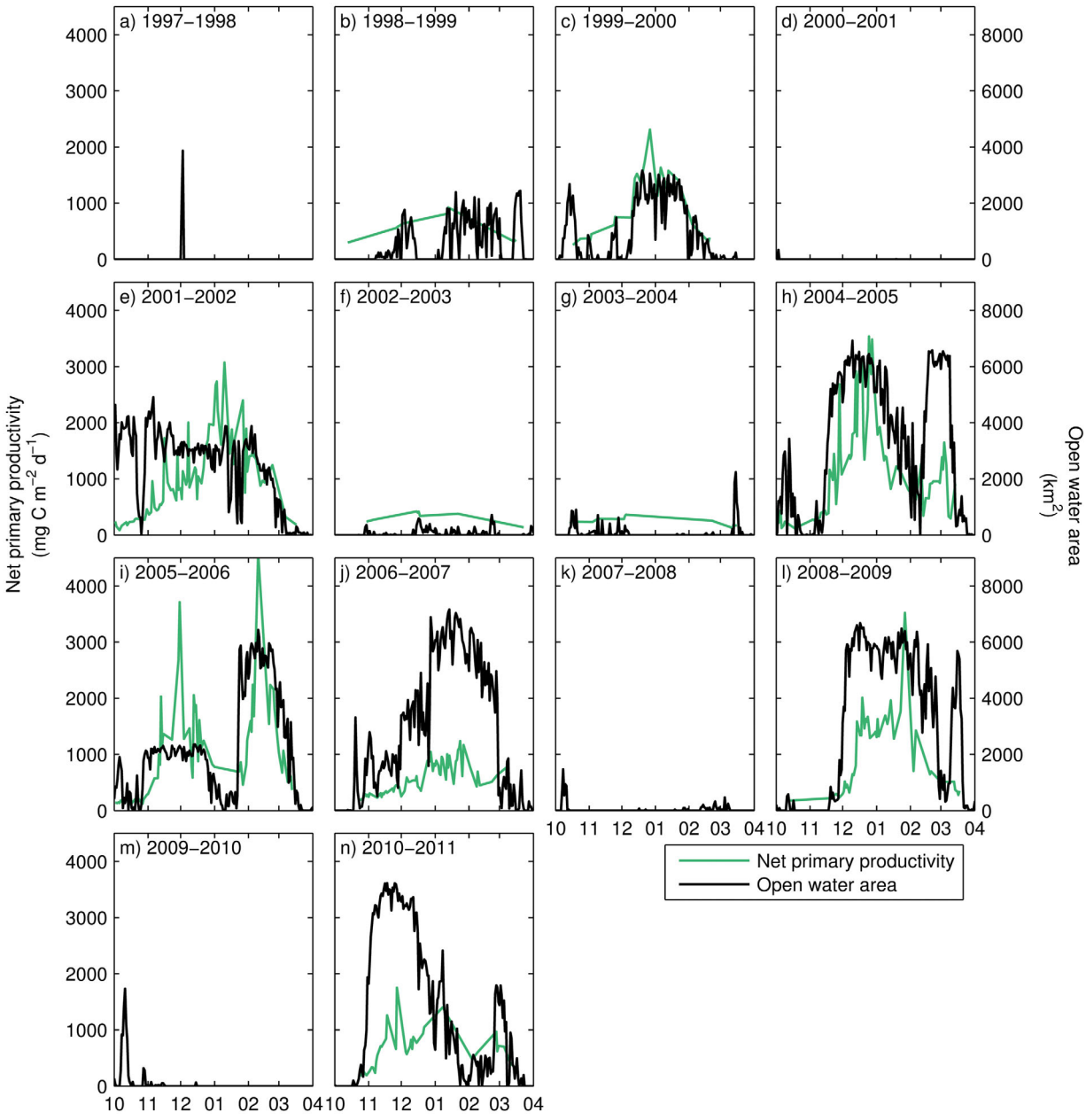

Figure 3. Same as Figure 2 for the Larsen B embayment.

in open water area (e.g., 2005–2006). Temporal patterns in the Larsen B largely resemble those of the Larsen A, with high interannual variability and coincident peaks and troughs in open water area. One exception occurred in 2002–2003, when the Larsen A and the rest of the NW Weddell Sea opened later in the season but the Larsen B did not (Figure 3). There is no significant trend in open water area over the length of the time series ($t_{(12)} = 1.54$, $p = 0.15$), although a general increase is notable between 1997 and 2005 due to the collapse of the remaining ice shelf. There is also no relationship between mean open water area and opening date ($\rho(8) = -0.32$, $p = 0.37$), unlike the Larsen A.

3.1.2. Spatial Patterns

[24] The dominant cross and along-shore patterns of seasonal open water appear in Figure 4. Duration and extent of open water in the NW Weddell as a whole is severely constrained, with ice cover persisting beyond the shelf break between October 1 and March 31 in most years. The longest open water season overall occurred in 2001–2002, when the whole region experienced ice-free conditions lasting over 140 days. Periods of open water exceeding 60 days are generally constrained to the Larsen embayments as well as south along the Larsen C ice shelf and north of James Ross Island. This is in sharp contrast to the WAP, where ice-free conditions persist for >160 days in most years apart from south of Anvers Island.

[25] Open water duration is comparable between the Larsen A and B when considering averages within the embayments (Table 1). Overall maximum open water is found within the embayment rather than offshore, where ice cover is less variable and more extensive (Figure 4). On

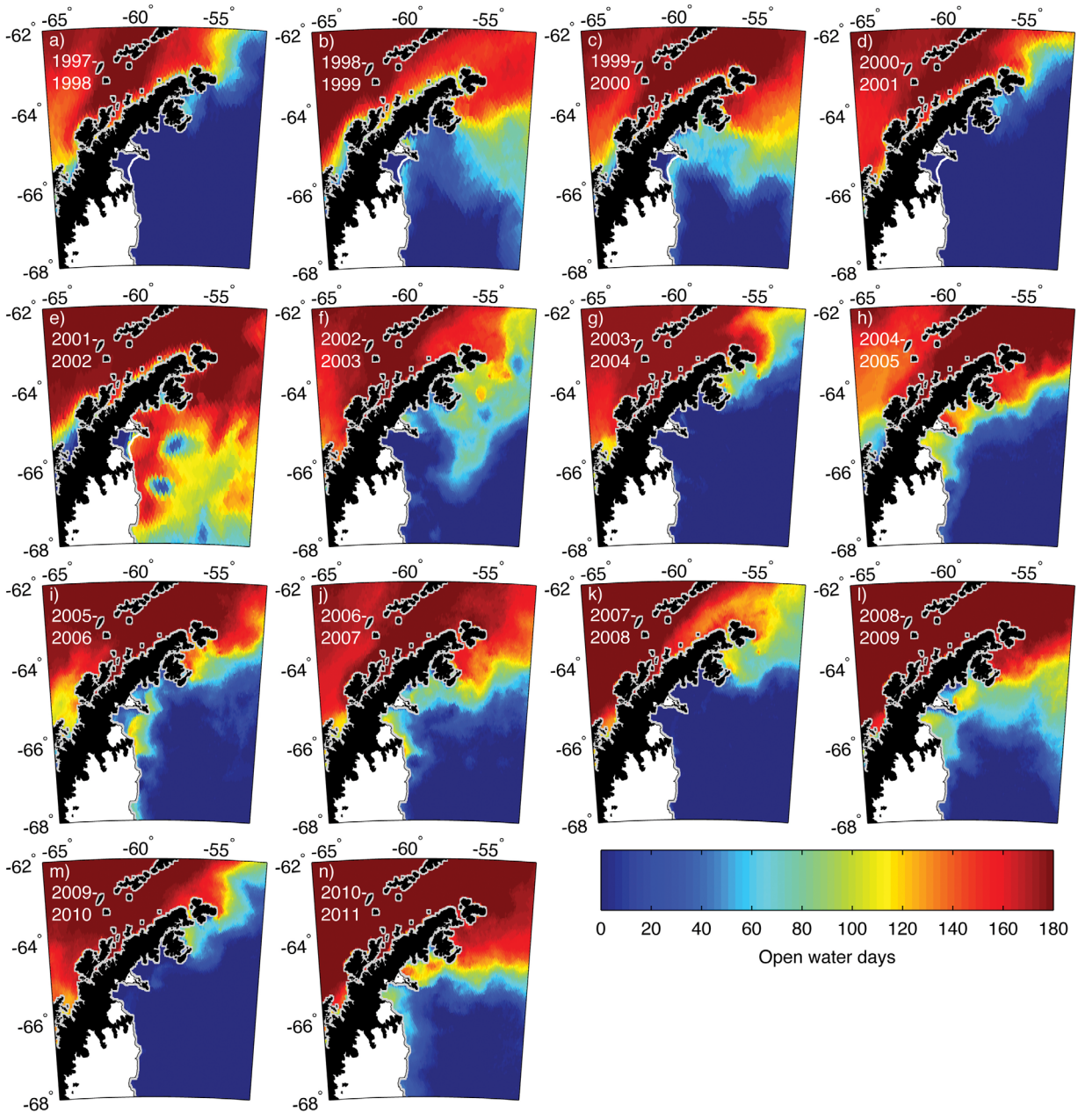

Figure 4. Number of open water days, defined as the number of days between 1 October and 31 March of each season when sea ice concentration in each pixel fell below the 40% threshold for SSM/I and 15% threshold for AMSR-E. Pixels within 7 km of the coast have been masked due to potential contamination. The white contour within the Larsen B embayment in (a-e) represents the ice shelf extent prior to the 2002 collapse.

average, open water conditions extend approximately 200–300 km offshore on the leeward side of the peninsula. However, open water within these regions is not spatially coherent and highly variable on an interannual basis. While ice-free conditions persist embayment-wide in some years (e.g., 1999–2000 in the Larsen A), they can also be restricted to the southern portions of the embayments. For example, open water lasted upward of 160 days offshore of the Drygalski Glacier in the Larsen A during the 2004–2005 season, while areas farther north saw a significantly shorter ice-free season. A similar pattern appears in the Larsen B in 2006–2007, when coastal waters adjacent to the SCAR Inlet, the remaining portion of the Larsen B ice shelf, stayed open for 120 days while areas farther north and offshore stayed ice free for a maximum of 60 days. In other years, ice-free conditions were restricted offshore near the mouth of the embayments. This occurred both prior to the breakup of the Larsen B (e.g., 1999–2000), but also in subsequent years in both embayments potentially due to the presence of fast ice occupying a configuration similar to that of the former ice shelves (e.g., 2005–2006).

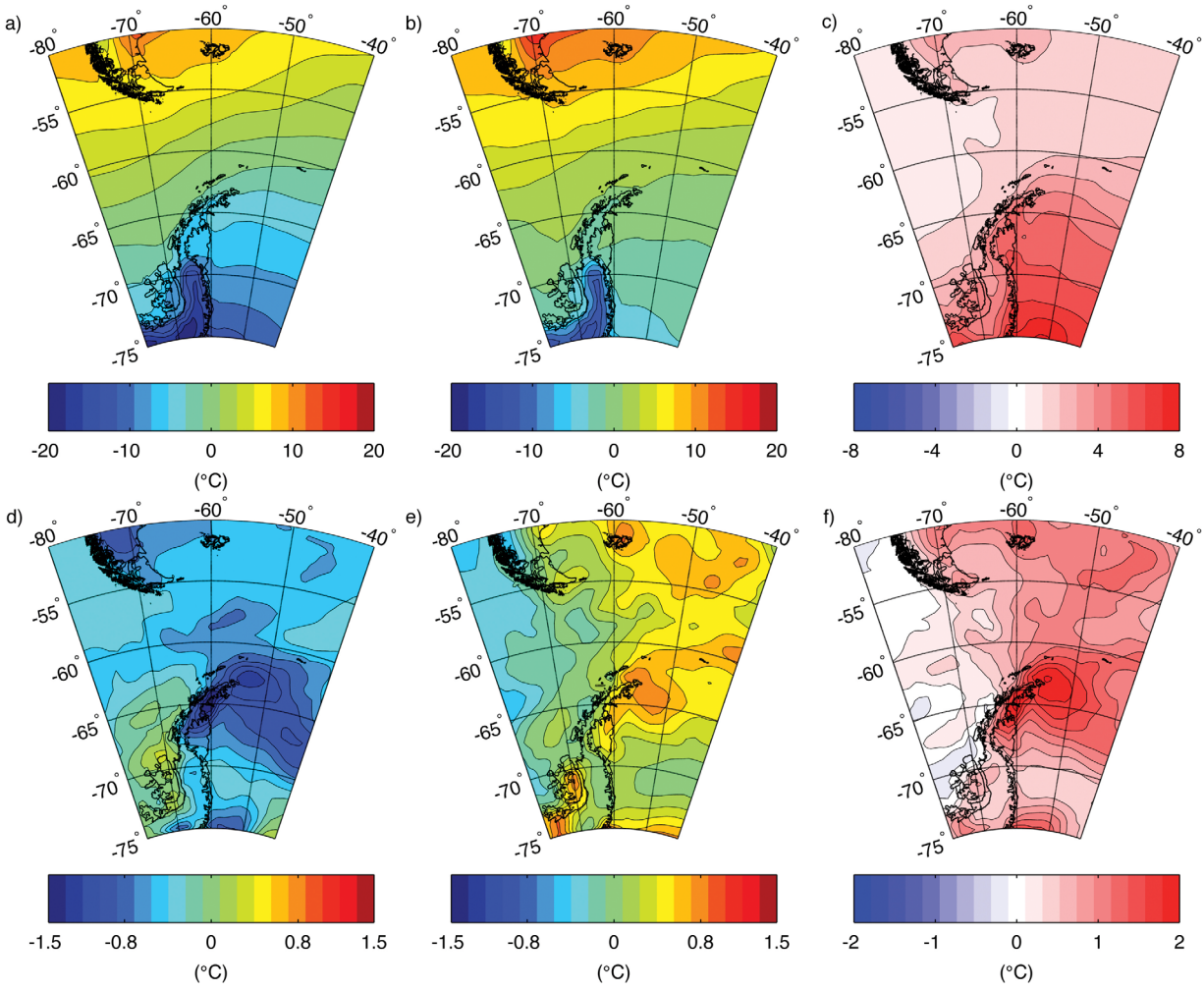

Figure 5. Mean monthly surface (2 m) air temperature (°C) composites for the 8 months with the (a) lowest and (b) highest open water areas in the Larsen embayments between 1997 and 2011; (c) difference in surface temperature composites between the high and low open water periods. (d–f) Same as Figures 5a–5c for composites of monthly surface air temperature anomalies for (d) low and (e) high open water periods, and (f) the difference between composites. Anomalies are calculated by subtracting the monthly 1997–2011 mean from each monthly data set.

3.2. Climate-Atmosphere-Ice Covariability

[26] Monthly surface (2 m) air temperature composites indicate that the NW Weddell Sea tends to be dominated by a different climate regime than the western side of the AP, but that in months with high open water area the maritime climate of the WAP impinges on the northeastern tip of the peninsula leading to higher average monthly temperatures near the freezing point (Figures 5a and 5b). The strongest warming signal is focused on the eastern side of the peninsula in the Weddell Sea (Figure 5c). Composites of surface air temperature anomaly further confirm that a significant temperature difference exists between months of high and low open water area, and that this difference is asymmetrical about the Antarctic Peninsula (Figures 5d–5f). Months of extensive open water correspond to warmer than usual temperatures along the northeastern AP, while months with low open water are associated with an average temperature anomaly of less than −1.5°C in the same region. This temperature anomaly difference of over 2°C is centered on the Larsen A and B embayments and extends

Table 3. The Eight October–March Months With the Highest and Lowest Open Water Areas for the Larsen Embayments Used in Creating Composites of ERA-Interim Data Sets[a]

High-Open Water	Date	Dec 2001	Dec 2004	Feb 2005	Jan 2005	Feb 2002	Nov 2001	Jan 2002	Feb 2003	Mean SAM Index
	SAM Index	1.16	**−1.02**	1.59	1.07	2.8	2.54	2.22	**−0.98**	1.1725
Low-Open Water	Date	Oct 1999	Dec 2000	Feb 2001	Mar 2001	Oct 2002	Oct 2007	Feb 2008	Feb 2010	Mean SAM Index
	SAM Index	**3.35**	−2.05	−2.7	−0.57	−5.77	−0.86	**1.09**	−2.12	−1.20375

[a]Bold SAM indices indicate departure from the general trend during high- and low-open water periods.

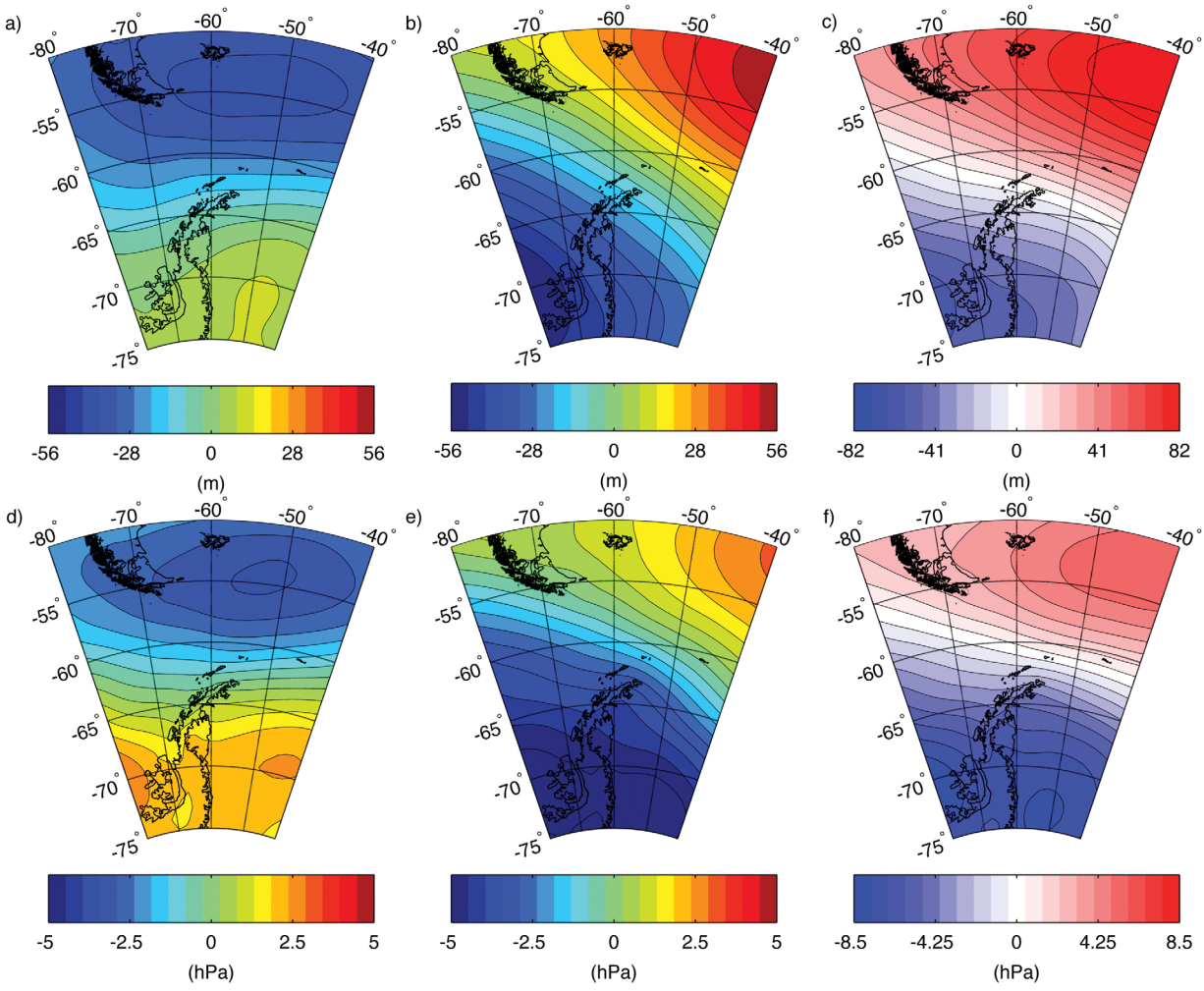

Figure 6. Mean monthly 500 hPa geopotential height (m) anomaly composites for the 8 months with the (a) lowest and (b) highest open water areas in the Larsen embayments between 1997 and 2011; (c) difference in mean monthly 500 hPa geopotential height anomaly between the high and low open water periods. (d–f) Same as Figures 6a–6c for sea level pressure (hPa) for the months with the (d) lowest and (e) highest open water areas; (f) differences between the composites.

north to the tip of the peninsula (Figure 5f). This is in contrast to the northwestern side of the barrier, where along the WAP only small differences in surface temperature anomaly are apparent. Thus to create this strong localization of the temperature anomaly, stronger sea to air sensible heat fluxes within the embayments likely play a role.

[27] Overall these surface temperature anomalies reflect broader changes in atmospheric properties that lead to increased advection of heat to the northeastern side of the peninsula. During months of high open water, the poleward gradients in sea level pressure and geopotential height at 500 hPa, which generate the polar westerlies, are stronger than during months of extensive ice cover in the embayments (Figure 6). The Amundsen Sea Low, a persistent feature in the Amundsen-Bellingshausen Sea sea level pressure, deepens during open water months while higher than usual sea level pressures dominate the South Atlantic. This results in strengthened polar westerlies with larger northerly component of the wind and an anomalous advection of warmer maritime air across the peninsula (Figures 7a–7c). These zonal anomalies in cross-peninsula winds extend southward over the Larsen C, but vanish beyond −70°S.

[28] Increased cross-peninsula winds during times of extensive open water in the embayments are also coupled with stronger vertical velocities on either side of the barrier, with negative (ascending) and positive (descending) wind anomalies along the WAP and EAP, respectively (Figures 7d–7f). These anomalies are focused north of −70°S and limited to within approximately 100 km of the coastline. Such conditions are consistent with the presence of föhn winds along the northeastern AP (see *van Lipzig et al*. [2008] and references therein). Stronger polar westerlies with an increased meridional component favor the orographic lifting of air masses above and across the peninsula rather than their deflection by the high and steep orography of the Antarctic Peninsula mountain range (flow over versus blocked conditions, respectively [*Orr et al*., 2004]). As air is lifted over the barrier its humidity and temperature decrease, gradually becoming denser than its surroundings.

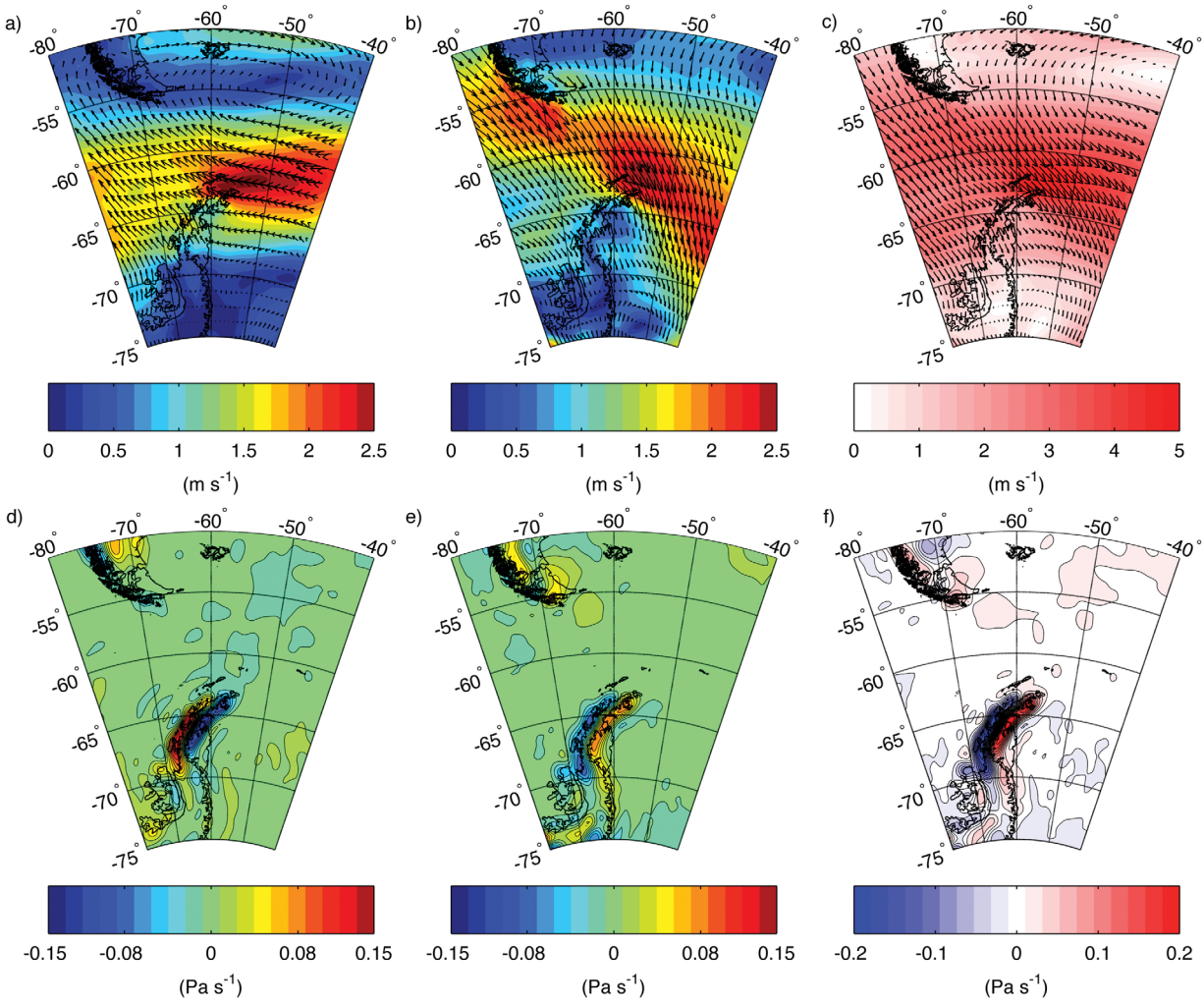

Figure 7. Same as in Figure 5 for anomalies in (a-c) surface (10 m) wind speed (m s^{-1}, shading) and velocity (arrows) and (d–f) vertical wind velocity at 850 hPa (Pa s^{-1}) for the months with (a and d) the lowest and (b and e) highest open water areas. Differences between the composites appear in Figures 7c and 7f.

On the leeward side, the air then sinks, warming adiabatically as it descends [*Beran*, 2013]. This increased air movement results in precipitation and cloud cover along the windward side and decreased cloud cover and dry, warm conditions on the leeward side. This mechanism, known as a föhn effect, therefore results from the interaction between synoptic-scale winds and the local topography of the Antarctic Peninsula. While föhn wind events cannot be resolved in the monthly reanalysis data set, the aforementioned patterns are consistent with increased flow-over conditions during months of low-ice cover.

[29] The months with highest (lowest) open water area used in our composites tended to have positive (negative) SAM index values (Table 3), suggesting a link between SAM and open water area in the embayments. When considering the whole monthly time series, we find a moderate positive relationship between SAM and open water area (Larsen A: $\rho(82) = 0.34$, $p < 0.01$; Larsen B: $\rho(82) = 0.38$, $p < 0.01$). There is, however, no significant relationship when considering seasonal averages for both variables (Larsen A: $\rho(12) = 0.23$, $p = 0.28$; Larsen B: $\rho(12) = 0.19$, $p = 0.39$). Using lagged correlations between seasonal open water area and a monthly SAM index smoothed with a 5 month running mean, we find instead a strong, significant relationship between mean October–March open water and a SAM index averaged over the preceding June–October (Larsen A: $\rho(12) = 0.60$, $p < 0.05$; Larsen B: $\rho(12) = 0.75$, $p < 0.01$; Figure 8).

3.3. Primary Production

3.3.1. Temporal Variability

[30] *Larsen A:* As in other parts of the Antarctic continental shelf, NPP remains low in October even during years of elevated open water area (e.g., 2001–2002), indicative of light limitation during austral spring (Figure 2) [*Vernet et al.*, 2012]. Rapid increases in NPP above the bloom threshold of 0.5 g C m^{-2} d^{-1} occur during November (on average November 26 ± 14.83 days) contingent upon the timing of sea ice retreat (Table 4). Although most studies along the Antarctic Peninsula have documented a January maximum in NPP rates, maximal values sometimes exceeding 3 g C m^{-2} d^{-1} occur between December and

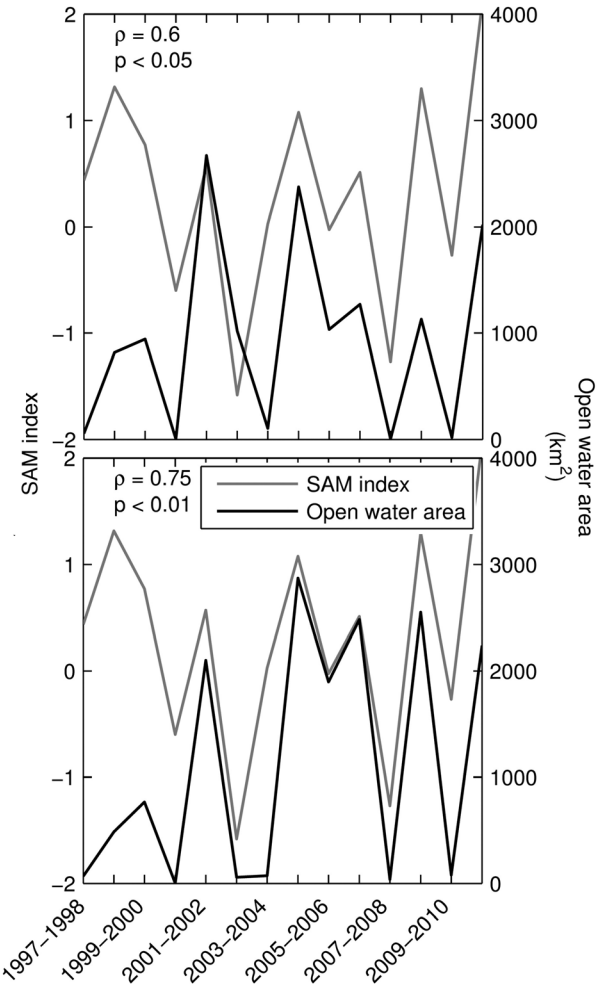

Figure 8. Time series of SAM index (black) and mean seasonal open water area (gray) for the (a) Larsen A and (b) Larsen B embayment. The monthly SAM index was smoothed with a 5 month running mean and lagged to find the most dominant cross correlations between SAM and open water area. The strongest correlation was found with SAM leading seasonal open water area by 5 months, corresponding to a June to October mean SAM index and an October to March mean open water.

late February in this embayment before a rapid decline below 0.5 g C m^{-2} d^{-1} in early fall (on average March 11 ± 7.71 days) even during years of extended open water (e.g., 2001–2002, 2008–2009). Duration of the phytoplankton bloom is inconsistent from year to year, lasting on average 67.36 ± 54.26 days. This is on average shorter than the duration of open water (87.43 days, Table 1), although the difference is not statistically significant ($p = 0.58$). Advance and retreat of sea ice within a season can lead to successive blooms and multiple peaks in NPP (e.g., 2005–2006, Figure 2). Overall the seasonal blooms are persistent, averaging 94.25 ± 8.27% over the 11 year record. Bloom duration is significantly correlated with open water duration ($\rho(12) = 0.95$, $p \ll 0.001$). However, there is no statistically significant temporal trend in bloom start date ($t_{(7)} = -0.68$, $p = 0.52$), end date ($t_{(7)} = -1.43$, $p = 0.20$) or duration ($t_{(12)} = 0.19$, $p = 0.85$) over this time span.

[31] Primary production in the embayment is highly variable on an interannual basis, with seasonal cycles in NPP apparent only during the years with an extended period of open water (Figure 2 and Table 2). Rates of daily depth-integrated productivity are high, averaging 806.26 ± 668.21 mg C m^{-2} d^{-1} over the length of the time series. Seasonally averaged NPP rates range from 0 (e.g., 2007–2008) to 1232 ± 870 mg C m^{-2} d^{-1} (e.g., 2001–2002, Table 2). Similarly, annual productivity averages 83.24 ± 67.07 g C m^{-2} yr^{-1}, with a low of 0 (e.g., 1997–1998) and a maximum of 200 g C m^{-2} yr^{-1} in 2001–2002 (Figure 9). These values are similar to the NW Weddell Sea as a whole, though the interannual variability is much greater due to the higher proportional year-to-year fluctuations in sea ice cover in the smaller embayments. Total primary production averages 0.195 ± 0.219 Tg C yr^{-1}, with a minimum of 0 (e.g., 1997–1998) and a maximum of 0.679 Tg C yr^{-1} in 2004–2005. On average the Larsen A accounts for 5.29 ± 4.49% of the calculated total production of the NW Weddell region while representing 4.68% of the surface area (Table 2). Annual and total NPP are positively correlated with open water duration ($\rho(12) = 0.89$, $p \ll 0.001$ and $\rho(12) = 0.91$, $p \ll 0.001$, respectively) as well as mean seasonal open water area ($\rho(12) = 0.82$, $p \ll 0.001$ and $\rho(12) = 0.90$, $p \ll 0.001$, respectively). Timing of embayment opening appears critical for primary production: both annual and total NPP are negatively correlated with day of opening of the embayment ($\rho(8) = -0.68$, $p < 0.05$ and $\rho(8) = -0.76$, $p < 0.05$). This is likely due to the strong negative relationship between timing of embayment opening and duration of open water conditions (see section 3.1.1 above).

[32] *Larsen B*: The seasonal cycle of primary production in the Larsen B embayment resembles that of the Larsen A (Figure 3). NPP increases above 0.5 g C m^{-2} d^{-1} generally occur in late November (November 18 ±12.73 days), reaching maximum values between November and January before decreasing below this threshold in March (March 4 ± 11.42 days, Table 4). Maximum rates of primary productivity can reach upward of 3 g C m^{-2} d^{-1}, with multiple peaks possible during a single season (e.g., 2005–2006). Over the length of the record, phytoplankton blooms last on average 60.93 ± 55.64 days, with multiple blooms tied to the advance and retreat of sea ice (Figure 3). As in the Larsen A, phytoplankton bloom duration is shorter than open water duration (61.64 versus 90.79 days, respectively, Tables 2 and 4), though the difference is not statistically significant ($p = 0.27$). Blooms are also persistent in years when open water conditions allow phytoplankton growth to occur (97.39 ± 6.10%), with bloom duration also positively correlated with open water duration ($\rho(12) = 0.91$, $p \ll 0.001$). There is no trend in bloom start date ($t_{(6)} = 0.84$, $p = 0.43$) or duration ($t_{(12)} = 0.51$, $p = 0.62$) over this time span. There is, however, a significant linear trend in bloom end date, with an observed increase of 2 days per year ($b = 2.0$ d yr^{-1}, $t_{(6)} = 2.65$, $p < 0.05$). This trend is dominated by changes occurring during the period of rapid ice shelf disintegration leading to the 2001–2002 season.

[33] Rates of daily primary productivity are high, averaging 825.82 ± 699.96 mg C m^{-2} d^{-1} and ranging from 0 to 1127 mg C m^{-2} d^{-1} when averaged seasonally (Table 2). Annual productivity is also extremely variable, with an alternating cycle of high and low productivity evident between 1997 and 2011 (Figure 9). Annual NPP

Table 4. Phytoplankton Bloom Characteristics for the Larsen A and B Embayments[a]

	Larsen A					Larsen B				
Year	Start (DOY)	End (DOY)	Duration (Days)	Bloom Days (Days)	Persistence (%)	Start (DOY)	End (DOY)	Duration (Days)	Bloom Days (Days)	Persistence (%)
1997–1998			0	0				0	0	
1998–1999	335	439	104	100	96	321	420	100	100	100
1999–2000	345	444	99	99	100	314	405	92	92	100
2000–2001			0	0				0	0	
2001–2002	315	442	127	116	91	316	428	113	113	100
2002–2003	355	427	72	71	99			0	0	
2003–2004			0	0	–			0	0	
2004–2005	320	443	123	121	98	324	439	115	111	97
2005–2006	316	432	117	117	100	310	436	126	126	100
2006–2007	323	431	108	81	75	340	432	92	76	83
2007–2008			0	0	–			0	0	
2008–2009	346	422	77	77	100	344	438	95	95	100
2009–2010			0	0				0	0	
2010–2011	322	438	116	103	89	313	433	120	120	100
Mean	330.78	435.33	67.36	63.21	94.25	322.75	428.88	60.93	59.50	97.39
SD	14.83	7.71	54.26	50.98	8.27	12.73	11.42	55.64	54.82	6.10

[a]Start and end dates follow the same year-day scheme as in Table 2.

averages 81.60 ± 68.06 g C m^{-2} yr^{-1} with a minimum of 0 (e.g., 1997–1998) and a maximum of 169 g C m^{-2} yr^{-1}, which is similar to both Larsen A and the NW Weddell Sea. While fluctuations in integrated primary productivity generally match dynamics in the Larsen A over the length of the record, an exception occurred in 2002–2003 when a lack of open water led to low seasonal productivity (Table 2 and Figure 3). Until the 2001–2002 austral summer season, a large portion of the Larsen B was still covered by ice shelf leading to reduced seasonal open water area and corresponding to years of lower total production than in the Larsen A. Following the 2002 disintegration of the ice shelf, total production surpassed that of the Larsen A due to the larger seasonal open water area and equal or higher rates of annual productivity (Table 2 and Figure 9). Total production was zero in 1997–1998, 2000–2001, 2007–2008, and 2009–2010 due to total sea ice cover and reached a maximum in 2004–2005 (0.818 Tg C yr^{-1}) when both open water area and annual primary productivity rate were at their maximum. Average total production between 1997 and 2011 is 0.254 ± 0.293 Tg C yr^{-1}. This represents 6.83 ± 7.89 % of the total calculated NW Weddell production, whereas the embayment represents 8.2% of the NW Weddell spatially. Like the Larsen A, annual and total NPP are positively correlated with open water duration ($\rho(12) = 0.89$, $p \ll 0.001$ and $\rho(12) = 0.88$, $p \ll 0.001$, respectively) as well as mean seasonal open water area ($\rho(12) = 0.79$, $p \ll 0.001$ and $\rho(12) = 0.91$, $p \ll 0.001$, respectively). Timing of embayment opening is correlated with annual primary production ($\rho(8) = -0.61$, $p < 0.10$), while total NPP shows no significant relationship with opening date ($\rho(8) = -0.45$, $p = 0.19$).

3.3.2. Spatial Variability

[34] There is a seasonally persistent cross-shelf gradient in daily integrated net primary productivity in both embayments in seasons of extensive open water. Monthly NPP along two onshore-offshore transects through the Larsen A and B during two productive seasons, 2001–2002 and 2004–2005, is depicted in Figures 10a–10d, with spatially averaged NPP for the entire time series appearing in Figure 10e.

[35] In the Larsen A, transects of NPP show a clear onshore-offshore gradient with low-productivity near the coast and relatively higher productivity 100–150 km offshore (Figures 10a and 10b). This gradient first becomes apparent in November during the rapid increases in overall NPP and often persists until February. A secondary decline in NPP is sometimes observed beyond 100 km. Daily integrated NPP is consistently lower inshore than offshore, where daily NPP rates reach upward of 4 g C m^{-2} d^{-1} in some instances. Variability in daily depth-integrated productivity is also higher offshore. The 2004–2005 austral summer exhibited the highest rates of NPP observed in the NW Weddell Sea between 1997 and 2011 with a maximum NPP of over 5.5 g C m^{-2} d^{-1} occurring 150 km offshore.

[36] A similar pattern is visible in the Larsen B, with a strong, persistent seasonal gradient present throughout most of the growing season. Until the final collapse in 2002, the remnant ice shelf prevented water column production within roughly 40 km of the coast (Figures 10c and 10d). Nevertheless, NPP still exhibited a strong cross-shore gradient, starting at the remnant ice shelf and increasing offshore [see *Domack et al.*, 2005]. This pattern moved shoreward in subsequent summer seasons after the ice shelf disintegrated. As in the Larsen A, rates of daily integrated primary productivity reach upward of 4 g C m^{-2} d^{-1} approximately 100 km offshore, with maximum rates during the 2004–2005 austral summer.

4. Discussion

[37] The once ice shelf-covered Larsen embayments now behave like polynyas [*Gordon and Comiso*, 1988]. Their opening is linked to föhn wind dynamics, whereby westerly winds impinging on the AP are forced over the peninsula, ultimately leading to warm (>0°C), dry winds blowing

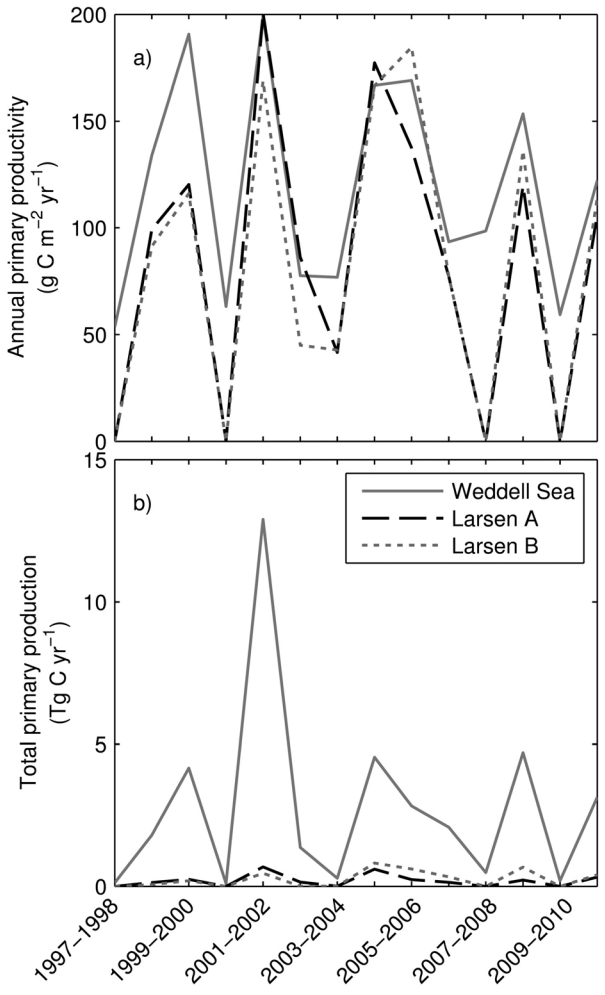

Figure 9. Time series of (a) annual primary productivity, calculated as the integral of daily primary productivity rates within the three regions of interest over March to October seasons, and (b) total annual production, calculated by multiplying daily productivity rates by open water area and integrating seasonally.

down the leeward side onto the coastal NW Weddell Sea (Figure 7) [*Orr et al*., 2008; *van Lipzig et al*., 2008]. As in coastal polynyas, the dynamic export of sea ice out of the embayment due to offshore winds likely plays a major role in open water dynamics. However, because of the warm nature of the winds, no new sea ice forms to provide the necessary sea to air heat flux common in latent heat polynyas. Instead, these regions behave much more like coastal sensible heat polynyas. In the traditional sense, the formation of sensible heat polynyas involves the transfer of heat from the ocean to the ice and atmosphere due to wind-driven convection of warm ($> -1.9°C$) water to the surface. In this case, the transfer of heat to the sea ice and surface ocean comes from the atmosphere due to the larger temperature gradient between air and sea. Warm surface air temperatures resulting from föhn winds, along with increased heat absorption in low-albedo surface waters during periods of increasing solar radiation, then prevent new ice growth in the embayments. This dynamic coupling between synoptic circulation, local topography, regional weather, and sea ice response make these polynyas unique on the scale of the Antarctic.

[38] Much like the Ross and Amundsen Sea polynyas, the Larsen A and B are seasonally productive regions with daily rates of primary productivity often exceeding 1 g C m^{-2} d^{-1} (Figures 2 and 3)[*Arrigo et al*., 2003]. Extensive open water is prominent only between October and March and sporadic during austral fall and winter (not shown), with large interannual variability in both spatial extent and duration (Figure 4). Phytoplankton growth is spatially restricted to a relatively narrow coastal area encompassing the embayments and occasionally a coastal lead extending below 66°S latitude along the Larsen C, with annually persistent sea ice offshore. As special cases of sensible heat polynyas, the Larsen embayments are sites of intense atmosphere-ice-ocean interaction linked to extensive biological activity. As seasonal hotspots of water column production in otherwise ice-covered coastal seas, these areas may therefore play a disproportionate role in the marine ecosystems of the NW Weddell Sea.

4.1. Physical Forcing and Atmosphere-Ice-Ocean Interactions

[39] The Antarctic Peninsula stretches farther north than any other part of the continental Antarctic, reaching subpolar latitudes near the South Shetland Islands, leading to a strong north/south climate gradient. Moreover, the tall arm of the Antarctic Peninsula constrains tropospheric circulation and separates the relatively warm, maritime climate on its western side from the cold continental climate of the Weddell Sea in the East [*Martin and Peel*, 1978; *King and Comiso*, 2003]. Due to these influences, the east coast of the peninsula is on average 7°C colder compared to similar latitudes on the western side, and its continental shelf tends to be covered by extensive annually persistent sea ice [*Kurtz and Markus*, 2012].

[40] The strengthening of the polar westerlies and increased frequency of flow-over conditions have been linked to higher incidence of surface melting along the ice shelves, which is thought to have contributed to their collapse [*Scambos et al*., 2000; *van den Broeke*, 2005]. We show here using ECMWF ERA-Interim reanalysis data sets that periods of low sea ice cover in the Larsen embayments are associated with stronger westerly winds and vertical wind velocities on either side of the AP north of −70°S (Figures 5–7). Increased advection of maritime air over the AP mountain range and the orographically forced downward motion on the leeward side leads to heating and drying of the air mass (föhn effect), favoring positive temperature and negative humidity anomalies over the Larsen A and B area as observed in the monthly ERA-Interim data set. Such conditions are conducive to both the melting and advection of sea ice along the northeast AP coastline. The spatial extent of the atmospheric warming from this study, approximately 200 km from the coast (Figure 5), matches that found by *van Lipzig et al*. [2008], who used a higher resolution model with 14 km grid spacing to study the relationship between SAM and surface temperature along the northeast AP. It also resembles the spatial extent of open water area on an interannual basis (Figure 4), indicating a potential link between this föhn mechanism and coastal Weddell ice cover. Higher monthly surface air temperature anomalies, as observed in our composites, are consistent with the

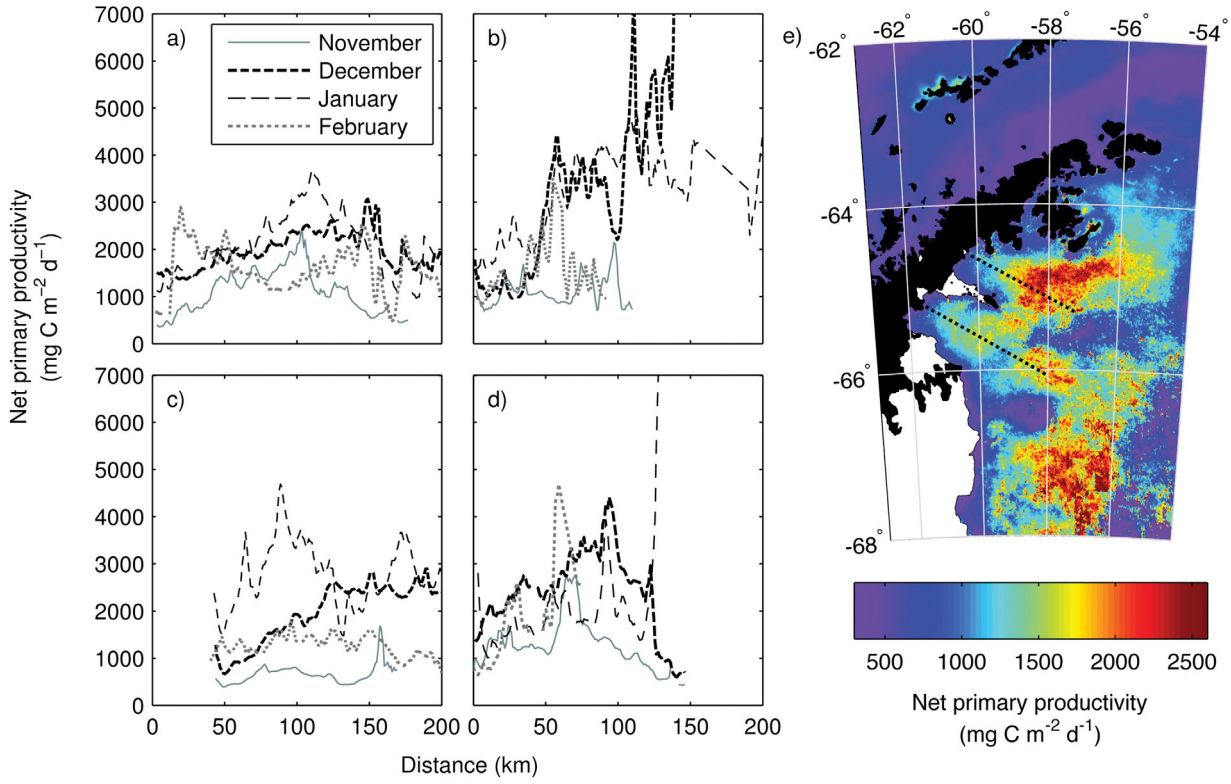

Figure 10. November–February, monthly cross-shelf transects of NPP through the Larsen A embayment in (a) 2001–2002 and (b) 2004–2005. Similar transects through the Larsen B for (c) 2001–2002 and (d) 2004–2005. (e) composite (average) of net primary productivity for the full 1997–2011 time series, showing location of transects from (a-d) (black dashed line). The origin corresponds to the Antarctic Peninsula coastline, with distance increasing offshore. Transect points are separated by 1 km and represent an average within a 3 × 3 pixel square along the transect. Lack of data within 40 km of the coastline in Figure 10c reflects the presence of the Larsen B ice shelf.

influence of the polar westerlies on the northeast AP and an increased frequency of föhn winds over the Larsen embayments during months of low ice cover [*Speirs et al*., 2013]. Because föhn winds persist on time scales of hours to several days [*Speirs et al*., 2010], the monthly anomaly data sets used here are, however, insufficient to resolve individual wind events and the underlying mechanism linking westerly winds and the timing of sea ice retreat and advance.

[41] The months with extensive open water used in our composites are associated with SAM+, and vice versa for ice-covered months (Table 3), indicating that both atmospheric conditions and sea ice are sensitive to the state of the SAM. The atmospheric patterns and links between large scale climate and regional atmospheric response described in this study are similar to those found in previous climate studies of the northeast Antarctic Peninsula [*Marshall et al*., 2006; *van Lipzig et al*., 2008].While the relationship between climate, atmosphere, ice and ocean presented here appears simple when considering composites based on extremes in open water area, we find only moderate month-to-month covariability between open water area and SAM over the full record and no relationship when correlating October–March averages. Instead, the strongest relationship is found between mean October and March open water area and a SAM index averaged over the preceding June–October (Figure 8). While the spring and summer seasons are most relevant in terms opening of the embayment and primary production, processes occurring during the winter may also have an impact on the physical structure of the sea ice. Sea ice in the Larsen embayments is likely composed of a mix of both land-fast ice and pack ice formed by the dynamical compaction of pack ice advected from the Weddell Gyre and the thermodynamic growth of ice in situ [*Fraser et al*., 2013]. While cold, quiescent periods as well as onshore winds during fall and winter months would favor rapid sea ice growth, high temperatures and increased wind stress caused by repeated offshore föhn wind events may serve to weaken the sea ice and precondition it for breakup in later months [*Arrigo et al*., 1998b; *Smith et al*., 1999; *Petrich et al*., 2012; *Fraser et al*., 2013].

[42] Regional weather patterns along the northeastern AP are sensitive to synoptic circulation as well as local dynamics via the topographic modification of westerly airflow (Figures 6 and 7). Furthermore, remote sensing and reanalysis data sets confirm that the region of the NW Weddell Sea showing the greatest atmospheric and sea ice response to changes in climate patterns encompasses the area having already undergone ice shelf breakup (Figures 4, 5, and 7). Comparatively little signal is apparent south toward the Larsen C ice shelf, as discussed in previous studies [*van Lipzig et al*., 2008]. Therefore, although we have shown that both Larsen A and B embayments have

experienced large increases in production and display intense sea ice dynamics, we do no expect similar changes to occur adjacent to the Larsen C unless the physical forcing on the ice shelf and coastal ocean changes.

4.2. Primary Production

[43] Intense phytoplankton blooms and extreme interannual variability characterizes primary production along the coastal NW Weddell Sea. Rates of daily integrated primary productivity are both very high and variable, averaging 806.26 ± 668.21 and 825.82 ± 699.96 mg C m^{-2} d^{-1} for the Larsen A and B, respectively (Table 2). These remote sensing estimates are comparable to other in situ measurements from the Weddell Sea. Using nutrient depletion in surface waters relative to the winter water, *Bertolin and Schloss* [2009] calculated a mean daily productivity rate of 426.54 ± 6.63 mg C m^{-2} d^{-1} for the Larsen A embayment in December 1996 following the breakup of the ice shelf. Other studies from the NW Weddell Sea reported rates of 570 to 1140 mg C m^{-2} d^{-1} offshore of the Larsen Ice Shelf [*Hoppema et al*., 2000] and 180 ± 440 mg C m^{-2} d^{-1} in a polynya identified along the Larsen C [*Arrigo and van Dijken*, 2003]. These rates are also similar to the Ross Sea, where average productivity rates ranging between 700 and 1820 mg C m^{-2} d^{-1} have been reported [*Smith et al*., 2011]. Individual seasons can be much more productive, reaching upward of 1232 mg C m^{-2} d^{-1} on average in 2001–2002. Averaged annual productivity rates of 86.36 g C m^{-2} yr^{-1} for the Larsen A and 79.27 g C m^{-2} yr^{-1} for the Larsen B further confirm that these are productive shelf regions of the Antarctic, as these rates exceed those reported for the Weddell Sea as a whole (70.2 g C m^{-2} yr^{-1}, [*Arrigo et al*., 2008a]) as well as Amundsen Sea and Pine Island polynyas (78.8 and 61.3 g C m^{-2} yr^{-1}, respectively [*Arrigo et al*., 2012]). These results are also higher than the annual primary productivity estimates for other Antarctic coastal polynyas [*Arrigo and van Dijken*, 2003]. Nevertheless, production in the Larsen A and B is characterized by a significantly shorter and much more variable phytoplankton growth season and open water duration than these other polynyas (Figures 2 and 3 and Table 2).

[44] Total production reaches a maximum of 0.68 Tg C yr^{-1} in the Larsen A and 0.82 Tg C yr^{-1} in the Larsen B (Table 2). These values primarily reflect the small size of the embayment rather than low levels of primary productivity, which can reach as high as 200 g C m^{-2} yr^{-1}. *Bertolin and Schloss* [2009] calculated a total annual production of only 0.07 Tg C yr^{-1} for their 1400 km^2 region of interest in the Larsen A, indicating that the embayment contributes less to the total Weddell Sea production than its spatial share of the region (0.015% of the mean Weddell Sea production and 0.05% of its surface area). *Peck et al*. [2010] provided another estimate of the contribution of new open water regions resulting from ice shelf breakup, using the annual productivity value of 176 g C m^{-2} yr^{-1} for Arthur Harbor in the WAP to estimate the size of the carbon pool in coastal waters uncovered following ice shelf retreat. Using this rate, the Larsen A and B would be expected to contribute 0.75 and 1.32 Tg C yr^{-1} of new organic carbon biomass, respectively. While the average rate of annual productivity used by *Peck et al*. [2010] is representative of productive seasons in the embayments, the study does not take into account sea ice dynamics when calculating total production, leading to a large overestimation of production on an interannual basis. The single season estimate by *Bertolin and Schloss* [2009] on the other hand underestimates total production in this region. Using a longer time series, we find that the embayments' contribution to production scales with their relative sizes (Table 2), though the exact percentage can vary drastically due to interannual variability in sea ice cover. This indicates that these regions contribute significantly to the overall production of the NW Weddell Sea.

4.2.1. Constraints on Production Estimates

[45] Our NPP data set gives insight into the development of the marine ecosystem following ice shelf collapse and serves as the first baseline of primary production for these new expanses of open ocean. Utilizing the large spatial and long temporal footprint of ocean color remote sensing, this study highlights the incredible variability of coastal primary production in the surface waters of the Larsen A and B embayments and the tight link between sea ice dynamics and phytoplankton growth. Limitations of remote sensing prevent the retrieval of data below clouds, near the ice edge and coastline, at depths beyond the reach of satellite sensors, and within and below the ice where high rates of primary productivity have also been measured [*Ackley et al*., 1979]. Algorithms used in calculating chl-a and NPP from satellite remote sensing reflectance have also been shown to underestimate these quantities in the Southern Ocean when compared to in situ data sets [*Arrigo et al*., 1998a; *Kahru and Mitchell*, 2010]. Parametrization of productivity models based on field campaigns and quantification of error is an active area of research [*Campbell et al*., 2002; *Carr et al*., 2006; *Johnson et al*., 2013; *Marrari et al*., 2006]. While in situ matchups are therefore critical to accurately estimate NPP, not enough are available in this region to ground truth our algorithm primarily due to the harsh weather and sea ice conditions that make the area largely inaccessible to research vessels. While these sources of error likely lead to an underestimate of NPP, the high rates of primary productivity presented in this study nevertheless demonstrate that the Larsen A and B are seasonally important sites of carbon fixation on par with the rest of the Weddell Sea, the most productive sea ice zone of the Antarctic [*Arrigo et al*., 2008a].

4.2.2. Ice-Production Covariability

[46] On average primary production increases gradually starting in November, peaking in January before rapidly decreasing in March, similar to growth patterns reported in the literature for other parts of the Antarctic. Yet the striking seasonal and interannual variability in open water area in the Larsen area limits production, leading to rates of annual and total primary production varying by three orders of magnitude (Table 2). Thus, although productivity is high, variability in sea ice cover is extreme on an interannual basis.

[47] There is no apparent linear trend in open water area nor in the timing of opening and closing over the 14 year record, as reported by *Stammerjohn et al*. [2012] and others, owing largely to extreme interannual variability but also to the relative short length of the time series. Similarly, there was no significant trend in primary production between 1997 and 2011 for either embayment, though

increases in both yearly and total NPP are notable in the Larsen B following the last major collapse during the 2001–2002 season. These results, and the relative synchrony between the two embayments, indicate that these previously ice shelf covered coastal marine ecosystems react rapidly to the removal of permanent ice cover, becoming productive as soon as open water is present, and that ensuing dynamics are highly dependent on atmosphere-ice-ocean interactions.

[48] Like other coastal polynyas, higher rates of phytoplankton primary productivity and longer phytoplankton blooms are associated with longer periods and larger extents of open water, indicating that NPP is sensitive to sea ice dynamics. Furthermore, NPP tends to be negatively correlated with date of opening of the embayment, with earlier openings associated with longer open water seasons and higher rates of productivity in the Larsen A. A similar trend is present in the Larsen B, though the relationship is weak due to the presence of the remnant ice shelf up until 2002 and two anomalous seasons during which the embayment opened early but closed only 3–5 days later (Figure 3 and Table 1). Nevertheless, this relationship runs contrary to what is observed in the sea ice zone along the WAP, where later sea ice retreat is associated with higher rates of primary productivity and phytoplankton biomass [*Vernet et al*., 2008]. There, later seasonal sea ice retreat is thought to lead to shallower mixed layer depths and stronger stratification during periods of increasing day length and sunlight, favoring higher NPP rates than in years of early retreat. This difference, as well as the strong correlation between NPP and open water area and duration, suggests that melting of retreating sea ice plays a comparatively minor role in stratifying the Larsen embayments, and that a relatively shallow and stable mixed layer is present when open water conditions persist.

4.2.3. Primary Production and Mixed Layer Depth

[49] In the Antarctic and elsewhere, mixed layer depth and the stability of the water column are important parameters thought to influence phytoplankton growth [*Hart*, 1934; *Sverdrup*, 1953; *Mitchell et al*., 1991]. While along the WAP the retreat of the ice edge in the spring and summer plays an important role in controlling the spatial distribution and magnitude of phytoplankton bloom on the shelf, the same relationship is not present along the eastern coastline of the AP. This may in part be due to the significant input of fresh water and ice from coastal glaciers. Removal of the Larsen A and B ice shelves has led to rapid and extensive mass losses in all the tributary glaciers feeding the embayments [*Scambos et al*., 2004; *Shuman et al*., 2011; *Berthier et al*., 2012], likely contributing to increased input of fresh water into these constrained coastal systems as both glacial melt and solid ice. This input of melt water into the surface ocean would serve to stabilize the mixed layer after sea ice retreat, while increased solar radiation during ice-free days could further intensify stratification by warming the summer mixed layer. Such conditions could in turn promote phytoplankton growth and high rates of primary productivity [*Smith and Nelson*, 1985, 1986; *Mitchell et al*., 1991; *Sakshaug et al*., 1991; *Lancelot et al*., 1993; *Dierssen et al*., 2002].

[50] Glacial and sea ice melt may also supply iron (Fe) to these waters [*Sedwick and DiTullio*, 1997; *Alderkamp et al*., 2012; *Gerringa et al*., 2012; *Lin and Twining*, 2012], which could help sustain the high rates of productivity. Although concentrations of Fe in coastal Antarctic waters are not thought to be limiting [*Martin et al*., 1990b], sustained production in similar polynya-like systems can be iron limited, particularly at the end of the growth season [*Sedwick et al*., 2000]. Glacial input of micronutrients into coastal waters may therefore serve to prolong phytoplankton bloom duration, primarily by pushing back the date of bloom decline. Further field studies are needed to explore the link between melt water dynamics and phytoplankton growth in the Larsen embayments and along the Antarctic Peninsula in general.

4.2.4. Spatial Patterns of Production

[51] While NPP rates and temporal patterns of bloom development observed along the EAP are comparable to the WAP, the spatial patterns of production are asymmetrical about the peninsula. Maximum values of primary productivity are found near the coast along the WAP, decreasing offshore to a low away from the continental shelf [*Vernet et al*., 2008]. In this study we observe a recurrent pattern of relatively low NPP near the coast increasing to a maximum 100–150 km offshore (Figure 10). Previous studies have noted similar patterns in other parts of the coastal Antarctic. A 2005 cruise to the Larsen B embayment noted low surface (7 m) chl-a biomass near the coast associated with relatively lower sea surface temperature and higher sea surface salinity (A. Leventer, personal communication). In the Mertz Glacier Region, a study found a deeper mixed layer near the Adelie Coast and increased stratification offshore which authors linked to atmospheric forcing [*Vaillancourt et al*., 2003]. Phytoplankton biomass in this case reached a maximum near-shore, though authors found evidence of deep mixing and downward advection of cells in this area, which they reasoned might lead to light limitation and over the long run limit production. In the Amundsen Sea, lower chl-a biomass near the Pine Island Glacier was coupled with deeper mixed layers [*Alderkamp et al*., 2012]. In this case, upwelling of Modified Circumpolar Deep Water (MCDW) at the ice shelf-water interface was implicated and thought to limit bloom formation nearshore.

[52] Depressed chl-a biomass and NPP near the coast in the Larsen embayments may be due to similar forcings, such as stronger wind stress on near shore waters leading to deeper mixed layers, or advection of surface waters offshore and coastal upwelling. Cold, offshore winds draining from the continent may also have a localized effect nearshore due to the decreasing strength of such winds offshore [*Bromwich and Kurtz*, 1984], leading to localized coastal convective mixing and sea ice formation. Regardless of the exact mechanisms, the cross-shelf pattern of production is a ubiquitous feature observed on daily, monthly, and seasonal time scales. If seasonally persistent throughout the euphotic zone, this gradient may have implication for sedimentation and the distribution of organic matter incorporated in the sediments.

4.3. Primary Production and Climate

[53] Despite relatively low average rates of annual net primary productivity, biological production in the Southern Ocean and the shelf areas around the continent plays an

important role in the drawdown of CO_2 into the deep ocean via the meridional overturning circulation [*Takahashi et al*., 2002, 2009; *Arrigo et al*., 2008b]. Recent studies have, however, identified a decreasing trend in carbon uptake in the Southern Ocean [*Wang and Moore*, 2012]. Because the Larsen A and B embayments were covered by ice shelves for the last 600 and 10,000 years, respectively [*Brachfeld et al*., 2003; *Domack et al*., 2005], photosynthetic activity in these areas represents new production and potentially a new sink for CO_2.

[54] *Bertolin and Schloss* [2009] noted intense photosynthetic activity driven mainly by diatoms coincident with $\%O_2$ supersaturation and depletion of CO_2 in surface waters during a 1996 cruise to the Larsen A, hypothesizing that the Larsen A could potentially be a site of seasonal carbon sequestration. We find that locally this new source of primary production is likely to serve as a significant carbon sink, but that the absolute magnitude of the carbon pool as estimated by total annual production is relatively low on the scale of the Antarctic due to the small size of the embayments and the high level of interannual variability (Table 2). The recent collapses of the Larsen A and B are representative of ongoing changes in ice shelf influenced systems taking place along the entire AP [*Cook and Vaughan*, 2010]. If the retreat of ice shelves continues along the Antarctic Peninsula and elsewhere in the Antarctic, we expect these new regions to be important sites of local and regional organic matter production and export.

4.4. Organic Matter Sedimentation and Spatial Patterns of Production

[55] Phytoplankton growth in the embayments marks a new source of organic matter to the marine ecosystem following ice shelf disintegration. Studies in the Ross Sea have indicated that advection of particulate organic carbon below ice shelves can lead to the establishment of thriving benthic communities [*Dayton and Oliver*, 1977]. In the case of the Larsen B, previous studies based on a 2006–2007 cruise to the Larsen embayments showed that significant organic matter export from the upper water column occurred only following the demise of the ice shelf with only limited input of advected organic matter [*Sane et al*., 2011a, 2011b, 2013; *Gutt et al*., 2011]. Their evidence included a marked change in the dominance of diatoms instead of sponge spicules in the sedimentary inventory of biogenic silica, significant increases in sediment pigment inventories and "fresh" organic matter based on phaeopigment to chlorophyll-a ratios, and increases in diatom frustules.

[56] Based on ^{14}C methods, the authors also calculated a sediment accumulation rate of 0.04 cm yr^{-1} following the collapse, which is very low compared to other glacially influenced coastal systems along the WAP [*Boldt et al*., 2013]. The stations sampled during this survey were, however, located close to the coast within the area last uncovered by the breakup in 2002, and may therefore receive less exported organic matter than offshore due to lower overall rates of overlying water column primary productivity (e.g., Figure 10). While three productive seasons occurred prior to their sampling (Table 2 and Figures 2 and 3), sea ice cover limited the length of the potential growth period in all seasons but 2004–2005 when the Larsen B embayment as a whole stayed open for upward of 120 days (Table 2 and Figure 4). In contrast, the longest open water season in 2005–2006 occurred at the mouth of the embayment rather than inshore. Spatial variability in both seasonal primary productivity and sea ice cover may therefore affect estimates of sedimentation rates and should be taken into account when looking at changes in organic matter export.

4.4.1. Implications for the Marine Ecosystem

[57] Benthic ecosystems are expected to experience a dramatic increase in the flux of organic matter to the sea floor as a consequence of this new water column production. Food availability via the spatially and temporally irregular export of particulate organic carbon from the euphotic zone can serve to structure benthic ecosystems [*Smith et al*., 2006; *McClintic et al*., 2008]. *Gutt et al*. [2011], examining benthic community composition and structure during a 2007 cruise, noted evidence of numerous deep-sea taxa at relatively shallow depths (300–800 m) within the Larsen A and B embayments, which they linked to the oligotrophic conditions prevailing prior to ice shelf collapse. They also noted that while the community composition of macro and megabenthic communities resembled that of non ice shelf covered Antarctic seafloor, species richness and density were lower than other parts of the Weddell Sea shelf. Distance from the former ice shelf edge was also found to be the single strongest environmental correlate with megabenthic community structure, giving further evidence that food availability is a primary factor structuring benthic communities in this region. As noted earlier, the relationship between phytoplankton growth and sea ice is highly dynamic in space and time, with strong cross-shelf gradients in phytoplankton production and extreme interannual variability in open water area which will affect the timing, quantity, and spatial distribution of organic matter export. Although studies from the WAP have shown that the link between overlying production and benthic ecosystems can be complex [*Smith et al*., 2006], we nevertheless expect that spatial and temporal variability in productivity within the embayments will have a large impact on the course of benthic ecosystem evolution, potentially leading to cross-shelf differences in benthic community characteristics mirroring gradients in production, seasonal open water, as well as the history of ice shelf retreat [see *Gutt et al*., 2013].

5. Conclusions

[58] Daily integrated rates of primary productivity in the embayments can be very high, reaching 1232 mg C m^{-2} d^{-1} in the Larsen A and 1127 mg C m^{-2} d^{-1} in the Larsen B on average during the most productive seasons. Much like in the West Antarctic Peninsula, phytoplankton blooms tend to start in November, reaching a peak in January before rapidly decreasing in March. NPP rates show a seasonally persistent cross-shelf gradient opposite that seen along the WAP, with low productivity inshore and maxima near the mouths of the embayments. Depression of NPP near the coast may be due to a deepening of the mixed layer associated with increased wind-driven mixing, sea ice formation, or upwelling, though the exact mechanism remains unclear. Maximum annual productivity rates of 200 and

184 g C m^{-2} yr^{-1} for the Larsen A and B, respectively, exceed those of other productive shelf waters of the Antarctic, including the Amundsen Sea and the Ross Sea. Yet the embayments are characterized by extreme interannual variability, with some years showing no measurable production due to the presence of sea ice.

[59] With the collapse of the Larsen A and B ice shelves, the newly uncovered embayments behave like seasonally productive polynyas. Primary production and sea ice dynamics are closely linked, with earlier embayment opening dates corresponding to longer growth seasons and higher productivity rates overall. Though open water dynamics are highly variable seasonally and interannually, opening of the embayments tends to occur in late October and closing in late March. Open water is limited to within 200–300 km of the coast, with annually persistent sea ice farther offshore in the Weddell Sea Gyre. The longest open water periods are confined to the southern portion of the embayments near the termini of major coastal glaciers and remnant ice shelves, though some years show maxima offshore due to the presence of a remnant ice shelf or fast ice occupying a similar configuration. With few exceptions, open water dynamics between the two embayments are remarkably similar indicating that a similar forcing is likely acting on the Larsen region north of 67°S.

[60] While the Weddell Sea generally experiences a cold, continental climate, months of extended open water tend to see a more maritime influence along the northeastern coast of the peninsula. Open water months tend to be associated with stronger westerly surface wind flow across the peninsula. Stronger polar westerlies are consistent with positive phases of SAM and the result of a deepening poleward pressure gradient, with negative anomalies in the Amundsen-Bellingshausen region and positive anomalies in the South Atlantic. Wind anomalies also correspond to positive temperature anomalies over the NW Weddell Sea centered on the Larsen A and B embayments. These patterns are consistent with a higher incidence of strong, downsloping föhn winds due to the topographic modification of oncoming westerly flow by the steep and tall orography of the peninsula. Because of the influence of these warm winds on the coastal NW Weddell, and the strong sea ice response, the embayments now appear to function as coastal sensible heat polynyas in which both the wind stress and large temperature difference between air and ice/ocean prevent sea ice growth. Though months of high (low) open water are overall associated with positive (negative) phases of SAM, we find only moderate correlation over the entire monthly time series and no correlation when considering seasonal (October–March) averages. Instead, mean October–March open water area is significantly correlated with average winter-early spring (June–October) SAM index. Periods of positive SAM and strong polar westerlies in the winter may lead to increased frequency of föhn winds, which may structurally weaken the sea ice and precondition it for breakup in the spring.

[61] There is no significant linear trend in either open water area or primary production over the 14 year time series, owing to the high interannual variability and relatively short length of the record. With the removal of ice shelves, these embayments have, however, quickly become productive regions of the Antarctic shelf, some years contributing more to total NPP than their spatial share of the NW Weddell Sea surface area. While the absolute magnitude of this new carbon pool is too low to contribute to carbon sequestration on a global scale and the interannual variability in production is extreme, the presence of this new organic matter in the water column and its sedimentation to the benthos are likely to lead to extensive changes in the regional marine ecosystem of the NW Weddell Sea.

[62] **Acknowledgments.** The authors thank the collaborators of the LARISSA project, particularly Arnold Gordon for thoughtful comments on polynya dynamics and Ted Scambos for discussions of föhn winds, Alison Cook for providing the historical ice shelf extent data set, the ocean color community for providing insight into data processing and analysis, and two reviewers for helpful comments on the manuscript. This work was supported by the National Science Foundation Office of Polar Programs under NSF grant ANT-0732983. MRC was also supported by the NSF Graduate Research Fellowship under grant DGE-1144086 and by NASA Headquarters under the NASA Earth and Space Science Fellowship Program—grant NNX12AN48H.

References

Ackley, S. F., and C. W. Sullivan (1994), Physical controls on the development and characteristics of Antarctic sea ice biological communities—A review and synthesis, *Deep Sea Res., Part I*, *41*(10), 1583–1604, doi:10.1016/0967-0637(94)90062-0.

Ackley, S. F., K. R. Buck, and S. Taguchi (1979), Standing crop of algae in the sea ice of the Weddell Sea region, *Deep Sea Res., Part A*, *26*(3), 269–281, doi:10.1016/0198-0149(79)90024-4.

Alderkamp, A.-C., M. M. Mills, G. L. van Dijken, P. Laan, C.-E. Thuróczy, L. J. Gerringa, H. J. de Baar, C. D. Payne, R. J. Visser, and A. G. Buma (2012), Iron from melting glaciers fuels phytoplankton blooms in the Amundsen Sea (Southern Ocean): Phytoplankton characteristics and productivity, *Deep Sea Res., Part II*, *71*, 32–48, doi:10.1016/j.dsr2.2012.03.005.

Andersen, S., R. Tonboe, L. Kaleschke, G. Heygster, and L. T. Pedersen (2007), Intercomparison of passive microwave sea ice concentration retrievals over the high-concentration Arctic sea ice, *J. Geophys. Res.*, *112*, C08004, doi:10.1029/2006JC003543.

Arrigo, K. R., and G. L. van Dijken (2003), Phytoplankton dynamics within 37 Antarctic coastal polynya systems, *J. Geophys. Res.*, *108*(C8), 3271, doi:10.1029/2002JC001739.

Arrigo, K. R., A. M. Weiss, and W. O. Smith Jr. (1998a), Physical forcing of phytoplankton dynamics in the southwestern Ross Sea, *J. Geophys. Res.*, *103*(C1), 1007–1021, doi:10.1029/97JC02326.

Arrigo, K. R., D. Worthen, A. Schnell, and M. P. Lizotte (1998b), Primary production in Southern Ocean waters, *J. Geophys. Res.*, *103*(C8), 15,587–15,600, doi:10.1029/98JC00930.

Arrigo, K. R., G. L. van Dijken, and S. Bushinsky (2008a), Primary production in the Southern Ocean, 1997–2006, *J. Geophys. Res.*, *113*, C08004, doi:10.1029/2007JC004551.

Arrigo, K. R., G. van Dijken, and M. Long (2008b), Coastal Southern Ocean: A strong anthropogenic CO_2 sink, *Geophys. Res. Lett.*, *35*, L21602, doi:10.1029/2008GL035624.

Arrigo, K. R., K. E. Lowry, and G. L. van Dijken (2012), Annual changes in sea ice and phytoplankton in polynyas of the Amundsen Sea, Antarctica, *Deep Sea Res., Part II*, *71*, 5–15, doi:10.1016/j.dsr2.2012.03.006.

Behrenfeld, M., and P. Falkowski (1997), Photosynthetic rates derived from satellite-based chlorophyll concentration, *Limnol. Oceanogr.*, *42*(1), 1–20, doi:10.4319/lo.1997.42.1.0001.

Beran, D. W. (2013), Large amplitude Lee waves and Chinook winds, *J. Appl. Meteorol.*, *6*(5), 865–877, doi:10.1175/1520-0450(1967)006<0865:LALWAC>2.0.CO;2.

Berthier, E., T. A. Scambos, and C. A. Shuman (2012), Mass loss of Larsen B tributary glaciers (Antarctic Peninsula) unabated since 2002, *Geophys. Res. Lett.*, *39*, L13501, doi:10.1029/2012GL051755.

Bertolin, M. L., and I. Schloss (2009), Phytoplankton production after the collapse of the Larsen A Ice Shelf, Antarctica, *Polar Biol.*, *32*(10), 1435–1446–1446, doi:10.1007/s00300-009-0638-x.

Boldt, K. V., C. A. Nittrouer, B. Hallet, M. N. Koppes, B. K. Forrest, J. S. Wellner, and J. B. Anderson (2013), Modern rates of glacial sediment accumulation along a 15° S-N transect in fjords from the Antarctic

Peninsula to southern Chile, *J. Geophys. Res. Earth Surf.*, *118*, doi: 10.1002/jgrf.20145, in press.

Boyd, P. (2004), Ironing out algal issues in the Southern Ocean, *Science*, *304*(5669), 396–397, doi:10.1126/science.1092677.

Boyd, P. W., and M. J. Ellwood (2010), The biogeochemical cycle of iron in the ocean, *Nat. Geosci.*, *3*(10), 675–682, doi:10.1038/ngeo964.

Brachfeld, S., E. Domack, C. Kissel, C. Laj, A. Leventer, S. Ishman, R. Gilbert, A. Camerlenghi, and L. B. Eglinton (2003), Holocene history of the Larsen-A Ice Shelf constrained by geomagnetic paleointensity dating, *Geology*, *31*(9), 749–752, doi:10.1130/G19643.1.

Bromwich, D. H., and D. D. Kurtz (1984), Katabatic wind forcing of the Terra Nova Bay polynya, *J. Geophys. Res.*, *89*(C3), 3561–3572, doi:10.1029/JC089iC03p03561.

Campbell, J., et al. (2002), Comparison of algorithms for estimating ocean primary production from surface chlorophyll, temperature, and irradiance, *Global Biogeochem. Cycles*, *16*(3), 1035, doi:10.1029/2001GB001444.

Carr, M.-E., et al. (2006), A comparison of global estimates of marine primary production from ocean color, *Deep Sea Res., Part II*, *53*(5–7), 741–770, doi:10.1016/j.dsr2.2006.01.028.

Comiso, J. C., and C. L. Parkinson (2008), Arctic sea ice parameters from AMSR-E data using two techniques and comparisons with sea ice from SSM/I, *J. Geophys. Res.*, *113*, C02S05, doi:10.1029/2007JC004255.

Cook, A., A. Fox, D. Vaughan, and J. G. Ferrigno (2005), Retreating glacier fronts on the Antarctic Peninsula over the past half-century, *Science*, *308*(5721), 541–544, doi:10.1126/science.1104235.

Cook, A. J., and D. G. Vaughan (2010), Overview of areal changes of the ice shelves on the Antarctic Peninsula over the past 50 years, *Cryosphere*, *4*(1), 77–98, doi:10.5194/tc-4-77-2010.

Dayton, P. K., and J. S. Oliver (1977), Antarctic soft-bottom benthos in oligotrophic and eutrophic environments, *Science*, *197*(4298), 55–58, doi:10.1126/science.197.4298.55.

Dierssen, H., M. Vernet, and R. Smith (2000), Optimizing models for remotely estimating primary production in Antarctic coastal waters, *Antarct. Sci.*, *12*(1), 20–32.

Dierssen, H., R. Smith, and M. Vernet (2002), Glacial meltwater dynamics in coastal waters west of the Antarctic peninsula, *Proc. Natl. Acad. Sci. U. S. A.*, *99*(4), 1790–1795, doi:10.1073/pnas.032206999.

Domack, E., D. Duran, A. Leventer, S. Ishman, S. Doane, S. McCallum, D. Amblas, J. Ring, R. Gilbert, and M. Prentice (2005), Stability of the Larsen B ice shelf on the Antarctic Peninsula during the Holocene epoch, *Nature*, *436*(7051), 681–685, doi:10.1038/nature03908.

Ferrigno, J. G., A. Cook, A. M. Mathie, R. J. Williams, C. Swithinbank, K. M. Foley, A. Fox, J. W. Thomson, and J. Sievers (2008a), Coastal-change and glaciological map of the Larsen Ice Shelf Area, Antarctica: 1940–2005, *U.S. Geol. Surv. Geol. Invest. Ser. Map I-2600-B*, (1 map sheet), 28 p. [Available at http://pubs.usgs.gov/imap/i-2600-b/.]

Ferrigno, J. G., A. J. Cook, K. M. Foley, R. S. Williams Jr., C. Swithinbank, A. Fox, J. W. Thomson, and J. Sievers (2008b), Coastal-change and glaciological map of the Trinity Peninsula area and South Shetland Islands, Antarctica—1843–2001, *U.S. Geol. Surv. Geol. Invest. Ser., Map I-2600-A*, 32 p. [Available at http://pubs.usgs.gov/imap/2600/A/.].

Fischer, G., R. Gersonde, and G. Wefer (2002), Organic carbon, biogenic silica and diatom fluxes in the marginal winter sea-ice zone and in the Polar Front Region: Interannual variations and differences in composition, *Deep Sea Res., Part II*, *49*(9–10), 1721–1745, doi:10.1016/S0967-0645(02)00009-7.

Fraser, A. D., R. A. Massom, K. J. Michael, B. K. Galton-Fenzi, and J. L. Lieser (2013), East Antarctic landfast sea ice distribution and variability, 2000–08, *J. Clim.*, *25*(4), 1137–1156, doi:10.1175/JCLI-D-10-05032.1.

Froneman, P. W., E. A. Pakhomov, and M. G. Balarin (2004), Size-fractionated phytoplankton biomass, production and biogenic carbon flux in the eastern Atlantic sector of the Southern Ocean in late austral summer 1997–1998, *Deep Sea Res., Part II*, *51*(22–24), 2715–2729, doi:10.1016/j.dsr2.2002.09.001.

Garibotti, I. A., M. Vernet, W. A. Kozlowski, and M. E. Ferrario (2003), Composition and biomass of phytoplankton assemblages in coastal Antarctic waters: A comparison of chemotaxonomic and microscopic analyses, *Mar. Ecol. Prog. Ser.*, *247*, 27–42, doi:10.3354/meps247027.

Gerringa, L. J. A., A.-C. Alderkamp, P. Laan, C.-E. Thuróczy, H. J. W. de Baar, M. M. Mills, G. L. van Dijken, H. V. Haren, and K. R. Arrigo (2012), Iron from melting glaciers fuels the phytoplankton blooms in Amundsen Sea (Southern Ocean): Iron biogeochemistry, *Deep Sea Res., Part II*, *71–76*(0), 16–31, doi:10.1016/j.dsr2.2012.03.007.

Glasser, N. F., T. A. Scambos, J. Bohlander, M. Truffer, E. Pettit, and B. J. Davies (2011), From ice-shelf tributary to tidewater glacier: Continued rapid recession, acceleration and thinning of Rohss Glacier following the 1995 collapse of the Prince Gustav Ice Shelf, Antarctic Peninsula, *J. Glaciol.*, *57*(203), 397–406.

Gordon, A. L., and J. C. Comiso (1988), Polynyas in the Southern Ocean, *Sci. Am.*, *258*(6), 90–97.

Gutt, J., et al. (2011), Biodiversity change after climate-induced ice-shelf collapse in the Antarctic, *Deep Sea Res., Part II*, *58*(1–2), 74–83, doi:10.1016/j.dsr2.2010.05.024.

Gutt, J., M. Cape, W. Dimmler, L. Fillinger, E. Isla, V. Lieb, T. Lundälv, and C. Pulcher (2013), Shifts in Antarctic megabenthic structure after ice-shelf disintegration in the Larsen area east of the Antarctic Peninsula, *Polar Biol.*, *36*(6), 895–906, doi:10.1007/s00300-013-1315-7.

Hart, T. J. (1934), On the phytoplankton of the southwest Atlantic and the Bellingshausen Sea, 1929–1931, *Discovery Rep.*, *8*, 1–286.

Hoppema, M., L. Goeyens, and E. Fahrbach (2000), Intense nutrient removal in the remote area off Larsen Ice Shelf (Weddell Sea), *Polar Biol.*, *23*(2), 85–94, doi:10.1007/s003000050012.

Johnson, R., P. G. Strutton, S. W. Wright, A. McMinn, and K. M. Meiners (2013), Three improved satellite chlorophyll algorithms for the Southern Ocean, *J. Geophys. Res. Oceans*, *118*, 3694–3703, doi:10.1002/jgrc.20270.

Kahru, M., and B. G. Mitchell (2010), Blending of ocean colour algorithms applied to the Southern Ocean, *Remote Sens. Lett.*, *1*(2), 119–124, doi:10.1080/01431160903547940.

Kaleschke, L., G. Heygster, C. Lupkes, A. Bochert, H. J. Hartmann, J. Haarpaintner, and T. Vihma (2001), SSM/I sea ice remote sensing for mesoscale ocean-atmosphere interaction analysis, *Can. J. Remote Sens.*, *27*(5), 526–537.

Kern, S., G. Spreen, L. Kaleschke, S. de La Rosa, and G. Heygster (2007), Polynya signature simulation method polynya area in comparison to AMSR-E 89 GHz sea-ice concentrations in the Ross Sea and off the Adelie Coast, Antarctica, for 2002–2005: First results, *Ann. Glaciol.*, *46*(1), 409–418, doi:10.3189/172756407782871585.

King, J. C., and J. C. Comiso (2003), The spatial coherence of interannual temperature variations in the Antarctic Peninsula, *Geophys. Res. Lett.*, *30*(2), 1040, doi:10.1029/2002GL015580.

Klinck, J. M. (1998), Heat and salt changes on the continental shelf west of the Antarctic Peninsula between January 1993 and January 1994, *J. Geophys. Res.*, *103*(C4), 7617–7636, doi:10.1029/98JC00369.

Kurtz, N. T., and T. Markus (2012), Satellite observations of Antarctic sea ice thickness and volume, *J. Geophys. Res.*, *117*, C08025, doi:10.1029/2012JC008141.

Lancelot, C., S. Mathot, C. Veth, and H. Baar (1993), Factors controlling phytoplankton ice-edge blooms in the marginal ice-zone of the northwestern Weddell Sea during sea ice retreat 1988: Field observations and mathematical modelling, *Polar Biol.*, *13*(6), 377–387, doi:10.1007/BF01681979.

Lin, H., and B. S. Twining (2012), Chemical speciation of iron in Antarctic waters surrounding free-drifting icebergs, *Mar. Chem.*, *128*, 81–91, doi:10.1016/j.marchem.2011.10.005.

Maaß, N., and L. Kaleschke (2010), Improving passive microwave sea ice concentration algorithms for coastal areas: Applications to the Baltic Sea, *Tellus, Ser. A*, *62*(4), 393–410, doi:10.1111/j.1600-0870.2010.00452.x.

Marrari, M., C. Hu, and K. Daly (2006), Validation of SeaWiFS chlorophyll a concentrations in the Southern Ocean: A revisit, *Remote Sens. Environ.*, *105*(4), 367–375, doi:10.1016/j.rse.2006.07.008.

Marshall, G. J. (2003), Trends in the southern annular mode from observations and reanalyses, *J Clim.*, *16*(24), 4134–4143, doi:10.1175/1520-0442(2003)016<4134:TITSAM>2.0.CO;2.

Marshall, G. J., A. Orr, N. P. M. van Lipzig, and J. C. King (2006), The impact of a changing southern hemisphere annular mode on Antarctic peninsula summer temperatures, *J. Clim.*, *19*(20), 5388–5404, doi:10.1175/JCLI3844.1.

Martin, J. H., R. M. Gordon, and S. E. Fitzwater (1990a), Iron in Antarctic waters, *Nature*, *345*(6271), 156–158, doi:10.1038/345156a0.

Martin, J. H., S. E. Fitzwater, and R. M. Gordon (1990b), Iron deficiency limits phytoplankton growth in Antarctic waters, *Global Biogeochem. Cycles*, *4*(1), 5–12, doi:10.1029/GB004i001p00005.

Martin, P. J., and D. A. Peel (1978), The spatial distribution of 10 m temperatures in the Antarctic Peninsula, *J. Glaciol.*, *20*, 311–317.

McClintic, M. A., D. J. DeMaster, C. J. Thomas, and C. R. Smith (2008), Testing the FOODBANCS hypothesis: Seasonal variations in near-bottom particle flux, bioturbation intensity, and deposit feeding based on

Th-234 measurements, *Deep Sea Res., Part II*, *55*(22–23), 2425–2437, doi:10.1016/j.dsr2.2008.06.003.

Mitchell, B. G., E. A. Brody, O. Holm-Hansen, C. McClain, and J. Bishop (1991), Light limitation of phytoplankton biomass and macronutrient utilization in the Southern Ocean, *Limnol. Oceanogr.*, *36*(8), 1662–1677.

Montes-Hugo, M., S. C. Doney, H. W. Ducklow, W. Fraser, D. Martinson, S. E. Stammerjohn, and O. Schofield (2009), Recent changes in phytoplankton communities associated with rapid regional climate change along the western Antarctic peninsula, *Science*, *323*(5920), 1470–1473, doi:10.1126/science.1164533.

O'Reilly, J. E., S. Maritorena, B. G. Mitchell, D. A. Siegel, K. L. Carder, S. A. Garver, M. Kahru, and C. McClain (1998), Ocean color chlorophyll algorithms for SeaWiFS, *J. Geophys. Res.*, *103*(C11), 24937–24953, doi:10.1029/98JC02160.

O'Reilly, J. E., et al. (2000), Ocean color chlorophyll a algorithms for SeaWiFS, OC2 and OC4: Version 4, *SeaWiFS Postlaunch Calibr. Valid. Anal.*, *11*(3), 8–22.

Orr, A., D. Cresswell, G. Marshall, J. Hunt, J. Sommeria, C. Wang, and M. Light (2004), A ''low-level'' explanation for the recent large warming trend over the western Antarctic Peninsula involving blocked winds and changes in zonal circulation, *Geophys. Res. Lett.*, *31*, L06204, doi:10.1029/2003GL019160.

Orr, A., G. J. Marshall, J. C. R. Hunt, J. Sommeria, C.-G. Wang, N. P. M. van Lipzig, D. Cresswell, and J. C. King (2008), Characteristics of summer airflow over the Antarctic Peninsula in response to recent strengthening of westerly circumpolar winds, *J. Atmos. Sci.*, *65*(4), 1396–1413, doi:10.1175/2007JAS2498.1.

Peck, L. S., D. K. A. Barnes, A. J. Cook, A. H. Fleming, and A. Clarke (2010), Negative feedback in the cold: Ice retreat produces new carbon sinks in Antarctica, *Global Change Biol.*, *16*(9), 2614–2623, doi:10.1111/j.1365-2486.2009.02071.x.

Petrich, C., H. Eicken, J. Zhang, J. Krieger, Y. Fukamachi, and K. I. Ohshima (2012), Coastal landfast sea ice decay and breakup in northern Alaska: Key processes and seasonal prediction, *J. Geophys. Res.*, *117*, C02003, doi:10.1029/2011JC007339.

Rott, H., P. Skvarca, and T. Nagler (1996), Rapid collapse of northern Larsen Ice Shelf, Antarctica, *Science*, *271*(5250), 788–792.

Rott, H., W. Rack, P. Skvarca, and H. De Angelis (2002), Northern Larsen Ice Shelf, Antarctica: Further retreat after collapse, *Ann. Glaciol.*, *34*, 277–282.

Sakshaug, E., D. Slagstad, and O. Holm-Hansen (1991), Factors controlling the development of phytoplankton blooms in the Antarctic Ocean: A mathematical model, *Mar. Chem.*, *35*(1–4), 259–271, doi:10.1016/S0304-4203(09)90021-4.

Sane, E., E. Isla, A. Gremare, J. Gutt, G. Vetion, and D. J. DeMaster (2011a), Pigments in sediments beneath recently collapsed ice shelves: The case of Larsen A and B shelves, Antarctic Peninsula, *J. Sea Res.*, *65*(1), 94–102, doi:10.1016/j.seares.2010.07.005.

Sane, E., E. Isla, A. M. Pruski, M. A. Barcena, G. Vetion, and D. DeMaster (2011b), Diatom valve distribution and sedimentary fatty acid composition in Larsen Bay, Eastern Antarctica Peninsula, *Cont. Shelf Res.*, *31*(11), 1161–1168, doi:10.1016/j.csr.2011.04.002.

Sane, E., E. Isla, D. Gerdes, A. Montiel, and J. M. Gili (2012), Benthic macrofauna assemblages and biochemical properties of sediments in two Antarctic regions differently affected by climate change, *Cont. Shelf Res.*, *35*, 53–63, doi:10.1016/j.csr.2011.12.008.

Sane, E., E. Isla, M. Angeles Barcena, and D. J. DeMaster (2013), A shift in the biogenic silica of sediment in the Larsen B continental shelf, off the eastern Antarctic Peninsula, resulting from climate change, *PLoS ONE*, *8*(1), e52632, doi:10.1371/journal.pone.0052632.

Scambos, T. A., C. Hulbe, M. Fahnestock, and J. Bohlander (2000), The link between climate warming and break-up of ice shelves in the Antarctic Peninsula, *J. Glaciol.*, *46*(154), 516–530, doi:10.3189/172756500781833043.

Scambos, T. A., C. Hulbe, and M. Fahnestock (2003), Climate-induced ice shelf disintegration in the Antarctic Peninsula, in *Antarctic Peninsula Climate Variability: Historical and Paleoenvironmental Perspectives*, edited by E. Domack et al., pp. 79–92, AGU, Washington, D. C., doi:10.1029/AR079p0079.

Scambos, T. A., J. A. Bohlander, C. A. Shuman, and P. Skvarca (2004), Glacier acceleration and thinning after ice shelf collapse in the Larsen B embayment, Antarctica, *Geophys. Res. Lett.*, *31*, L18402, doi:10.1029/2004GL020670.

Scambos, T. A., T. M. Haran, M. A. Fahnestock, T. H. Painter, and J. Bohlander (2007), MODIS-based Mosaic of Antarctica (MOA) data sets: Continent-wide surface morphology and snow grain size, *Remote Sens. Environ.*, *111*(2–3), 242–257, doi:10.1016/j.rse.2006.12.020.

Sedwick, P. N., and G. R. DiTullio (1997), Regulation of algal blooms in Antarctic Shelf Waters by the release of iron from melting sea ice, *Geophys. Res. Lett.*, *24*(20), 2515–2518, doi:10.1029/97GL02596.

Sedwick, P. N., G. R. DiTullio, and D. J. Mackey (2000), Iron and manganese in the Ross Sea, Antarctica: Seasonal iron limitation in Antarctic shelf waters, *J. Geophys. Res.*, *105*(C5), 11,321–11,336, doi:10.1029/2000JC000256.

Shadwick, E. H., S. R. Rintoul, B. Tilbrook, G. D. Williams, N. Young, A. D. Fraser, H. Marchant, J. Smith, and T. Tamura (2013), Glacier tongue calving reduced dense water formation and enhanced carbon uptake, *Geophys. Res. Lett.*, *40*, 904–909, doi:10.1002/grl.50178.

Shuman, C. A., E. Berthier, and T. A. Scambos (2011), 2001–2009 elevation and mass losses in the Larsen A and B embayments, Antarctic Peninsula, *J. Glaciol.*, *57*(204), 737–754, doi:10.3189/002214311797409811.

Skvarca, P., W. Rack, H. Rott, and T. I. Donángelo (1999), Climatic trend and the retreat and disintegration of ice shelves on the Antarctic Peninsula: An overview, *Polar Res.*, *18*(2), 151–157, doi:10.1111/j.1751-8369.1999.tb00287.x.

Smith, C. R., S. Mincks, and D. J. DeMaster (2006), A synthesis of benthopelagic coupling on the Antarctic shelf: Food banks, ecosystem inertia and global climate change, *Deep Sea Res., Part II*, *53*(8–10), 875–894, doi:10.1016/j.dsr2.2006.02.001.

Smith, R., et al. (1995), The Palmer LTER: A long-term ecological research program at palmer station, Antarctica, *Oceanography*, *8*(3), 77–86, doi:10.5670/oceanog.1995.01.

Smith, R. C., et al. (1999), Marine ecosystem sensitivity to climate change, *BioScience*, *49*(5), 393–404.

Smith, W. H. F., and D. T. Sandwell (1997), Global sea floor topography from satellite altimetry and ship depth soundings, *Science*, *277*(5334), 1956–1962.

Smith, W. O., and D. M. Nelson (1985), Phytoplankton bloom produced by a receding ice edge in the Ross Sea: Spatial coherence with the density field, *Science*, *227*(4683), 163–166, doi:10.1126/science.227.4683.163.

Smith, W. O., Jr., and D. M. Nelson (1986), Importance of ice edge phytoplankton production in the Southern Ocean, *BioScience*, *36*(4), 251–257, doi:10.2307/1310215.

Smith, W. O., V. Asper, S. Tozzi, X. Liu, and S. E. Stammerjohn (2011), Surface layer variability in the Ross Sea, Antarctica as assessed by in situ fluorescence measurements, *Prog. Oceanogr.*, *88*(1–4), 28–45, doi:10.1016/j.pocean.2010.08.002.

Speirs, J. C., D. F. Steinhoff, H. A. McGowan, D. H. Bromwich, and A. J. Monaghan (2010), Foehn winds in the McMurdo Dry Valleys, Antarctica: The origin of extreme warming events, *J. Clim.*, *23*(13), 3577–3598, doi:10.1175/2010JCLI3382.1.

Speirs, J. C., H. A. McGowan, D. F. Steinhoff, and D. H. Bromwich (2013), Regional climate variability driven by foehn winds in the McMurdo Dry Valleys, Antarctica, *Int. J. Climatol.*, *33*(4), 945–958, doi:10.1002/joc.3481.

Spreen, G., L. Kaleschke, and G. Heygster (2008), Sea ice remote sensing using AMSR-E 89-GHz channels, *J. Geophys. Res.*, *113*, C02S03, doi:10.1029/2005JC003384.

Stammerjohn, S., R. Massom, D. Rind, and D. Martinson (2012), Regions of rapid sea ice change: An inter-hemispheric seasonal comparison, *Geophys. Res. Lett.*, *39*, L06501, doi:10.1029/2012GL050874.

Stammerjohn, S. E., D. G. Martinson, R. C. Smith, and R. A. Iannuzzi (2008), Sea ice in the western Antarctic Peninsula region: Spatio-temporal variability from ecological and climate change perspectives, *Deep Sea Res., Part II*, *55*, 2041–2058, doi:10.1016/j.dsr2.2008.04.026.

Sverdrup, H. (1953), On conditions for the vernal blooming of phytoplankton, *J. Cons. Int. Explor. Mer.*, *18*(3), 287–295, doi:10.1093/icesjms/18.3.287.

Takahashi, T., et al. (2002), Global sea–air CO_2 flux based on climatological surface ocean pCO_2, and seasonal biological and temperature effects, *Deep Sea Res., Part II*, *49*(9–10), 1601–1622, doi:10.1016/S0967-0645(02)00003–6.

Takahashi, T., et al. (2009), Climatological mean and decadal change in surface ocean pCO(2), and net sea-air CO_2 flux over the global oceans, *Deep Sea Res., Part II*, *56*(8–10), 554–577, doi:10.1016/j.dsr2.2008.12.009.

Thompson, D. W. J. (2002), Interpretation of recent southern hemisphere climate change, *Science*, *296*(5569), 895–899, doi:10.1126/science.1069270.

Tréguer, P., and G. Jacques (1992), Dynamics of nutrients and phytoplankton, and fluxes of carbon, nitrogen and silicon in the Antarctic Ocean, *Polar Biol.*, *12*(2), 149–162, doi:10.1007/BF00238255.

Vaillancourt, R. D., R. N. Sambrotto, S. Green, and A. Matsuda (2003), Phytoplankton biomass and photosynthetic competency in the summertime Mertz Glacier Region of East Antarctica, *Deep Sea Res., Part II*, *50*(8–9), 1415–1440, doi:10.1016/S0967-0645(03)00077-8.

van den Broeke, M. (2005), Strong surface melting preceded collapse of Antarctic Peninsula ice shelf, *Geophys. Res. Lett.*, *32*, L12815, doi:10.1029/2005GL023247.

van den Broeke, M., D. van As, C. Reijmer, and R. van de Wal (2005), Sensible heat exchange at the Antarctic snow surface: A study with automatic weather stations, *Int. J. Climatol.*, *25*(8), 1081–1101, doi:10.1002/joc.1152.

van Lipzig, N. P. M., G. J. Marshall, A. Orr, and J. C. King (2008), The relationship between the southern hemisphere annular mode and Antarctic Peninsula summer temperatures: Analysis of a high-resolution model climatology, *J. Clim.*, *21*(8), 1649–1668, doi:10.1175/2007JCLI1695.1.

Vaughan, D. G., and C. S. M. Doake (1996), Recent atmospheric warming and retreat of ice shelves on the Antarctic Peninsula, *Nature*, *379*(6563), 328–331, doi:10.1038/379328a0.

Vernet, M., D. Martinson, R. Iannuzzi, S. Stammerjohn, W. Kozlowski, K. Sines, R. Smith, and I. Garibotti (2008), Primary production within the sea-ice zone west of the Antarctic Peninsula: I: Sea ice, summer mixed layer, and irradiance, *Deep Sea Res., Part II*, *55*, 2068–2085, doi:10.1016/j.dsr2.2008.05.021.

Vernet, M., W. A. Kozlowski, L. R. Yarmey, A. T. Lowe, R. M. Ross, L. B. Quetin, and C. H. Fritsen (2012), Primary production throughout austral fall, during a time of decreasing daylength in the western Antarctic Peninsula, *Mar. Ecol. Prog. Ser.*, *452*, 45–61, doi:10.3354/meps09704.

Walsh, J. J., D. A. Dieterle, and J. Lenes (2001), A numerical analysis of carbon dynamics of the Southern Ocean phytoplankton community: The roles of light and grazing in effecting both sequestration of atmospheric CO_2 and food availability to larval krill, *Deep Sea Res., Part I*, *48*(1), 1–48, doi:10.1016/S0967-0637(00)00032-7.

Wang, S., and J. K. Moore (2012), Variability of primary production and air-sea CO_2 flux in the Southern Ocean, *Global Biogeochem. Cycles*, *26*, GB1008, doi:10.1029/2010GB003981.